A derecho climatology (2004-2021) in the United States based on machine learning identification of bow echoes

Jianfeng Li[1, *], Andrew Geiss[1], Zhe Feng[1, *], L. Ruby Leung[1], Yun Qian[1], Wenjun Cui[2, 3]

[1]Atmospheric, Climate, and Earth Sciences Division, Pacific Northwest National Laboratory, Richland, Washington, USA

[2]Cooperative Institute for Severe and High-Impact Weather Research and Operations, University of Oklahoma, Norman, Oklahoma, USA

[3]National Severe Storms Laboratory, National Oceanic and Atmospheric Administration, Norman, Oklahoma, USA

*Correspondence to Jianfeng Li (jianfeng.li@pnnl.gov) and Zhe Feng (zhe.feng@pnnl.gov)

Abstract

Due to their persistent widespread severe winds, derechos pose significant threats to human safety and property, ~~and they are as hazardous and fatal as~~ with impacts comparable to many tornadoes and hurricanes. Yet, automated detection of derechos remains challenging due to the absence of spatiotemporally continuous observations and the complex criteria employed to define the phenomenon. ~~This study proposes~~This study presents an objective derecho detection approach capable of automatically identify derechos in both observations and model results. The approach is grounded in a physically based definition of derechos ~~that contains the key features of derechos described in the literature and allows their automated objective identification using either observations or model simulations. The automated detection is composed of~~and integrates three algorithms: (1) the Python Flexible Object Tracker (PyFLEXTRKR) algorithm to track mesoscale convective systems (MCSs), (2) a semantic segmentation convolutional neural network to identify bow echoes, and (3) a comprehensive classification algorithm to ~~classify MCSs as~~detect derechos ~~or~~ within MCS lifecycles and distinguish derecho-producing from non-derecho ~~events.~~ producing MCSs. Using ~~the new~~this approach, we develop a novel high-resolution (4 km and hourly) observational dataset of derechos and accompanying derecho-producing MCSs over the United States east of the Rocky Mountains from 2004 to 2021. The dataset consists of two subsets based on different gust speed data sources and is analyzed to document the ~~derecho~~ climatology of derechos in the United States. ~~Many more~~On average, 12-15 derechos ~~(increased by ~50-400%)~~ are identified ~~in the dataset (~31 events~~ per year~~) than in~~, aligning with previous estimations (~6-21 events ~~per year), but the~~annually). The spatial distribution and seasonal variation patterns ~~resemble earlier~~are consistent with prior studies ~~with a~~, showing peak ~~occurrence~~occurrences in the Great Plains and Midwest during the warm season. ~~In addition, around 20% of~~ Additionally, during the study period, derechos account for approximately 3.1% of measured damaging ~~gust~~gusts ($\geq$ 25.93 m s^{-1}) ~~reports are produced by derechos during the dataset period~~ over the eastern United States ~~east of the Rocky Mountains.~~. The dataset is

publicly available at ~~https://doi.org/10.5281/zenodo.10884046~~https://doi.org/10.5281/zenodo.14835362 (Li et al., ~~2024~~2025).

1 Introduction

A derecho is qualitatively defined as a widespread, long-lived straight-line windstorm associated with a fast-moving mesoscale convective system (MCS~~).~~), and the latter is named a derecho-producing MCS (DMCS). Figure 1 shows two of the most destructive derechos and their accompanying DMCSs in the United States: the June 2012 North American derecho and the August 2020 Midwest Derecho. Both events lasted for over 10 hours, with apparent bow echoes and extensive damaging wind gusts (≥ 25.93 m s^{-1}). Due to the persistent widespread damaging gusts, derechos can severely damage property and threaten human lives, as exemplified by the extensive power outages and more than ten fatalities caused by the two derechos. Ashley and Mote (2005) demonstrated that derechos could be as hazardous as and were comparable in ~~magnitude~~impact to most hurricanes and tornadoes in the United States between 1986 and 2003.

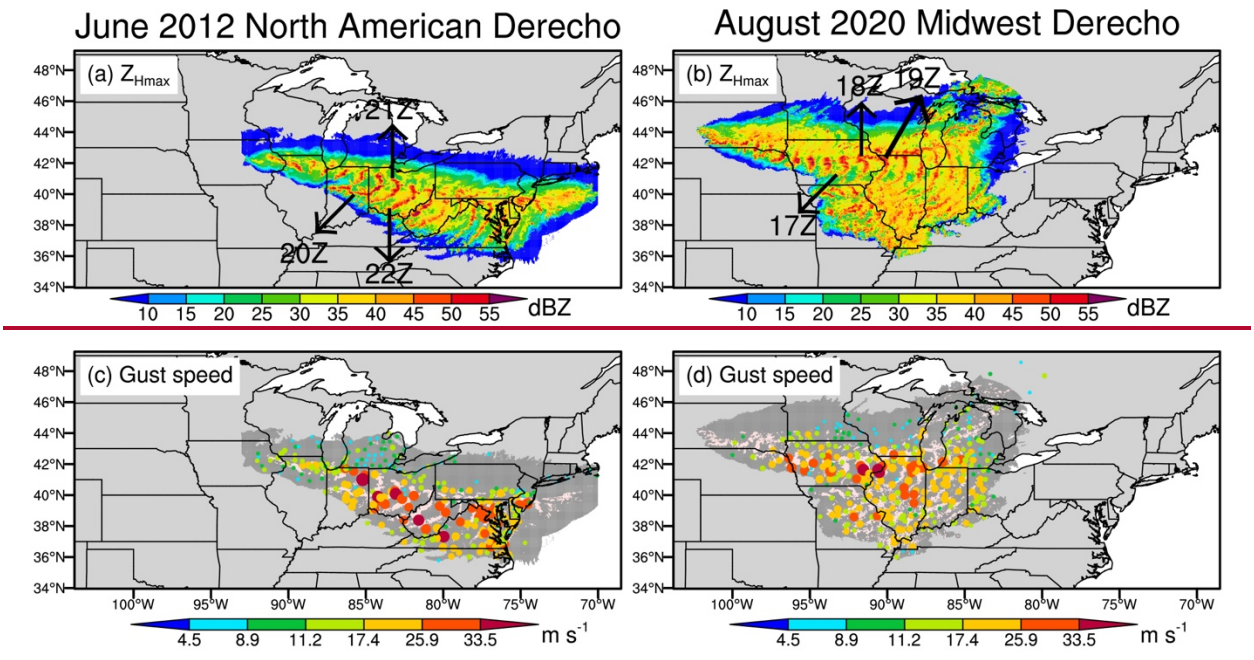

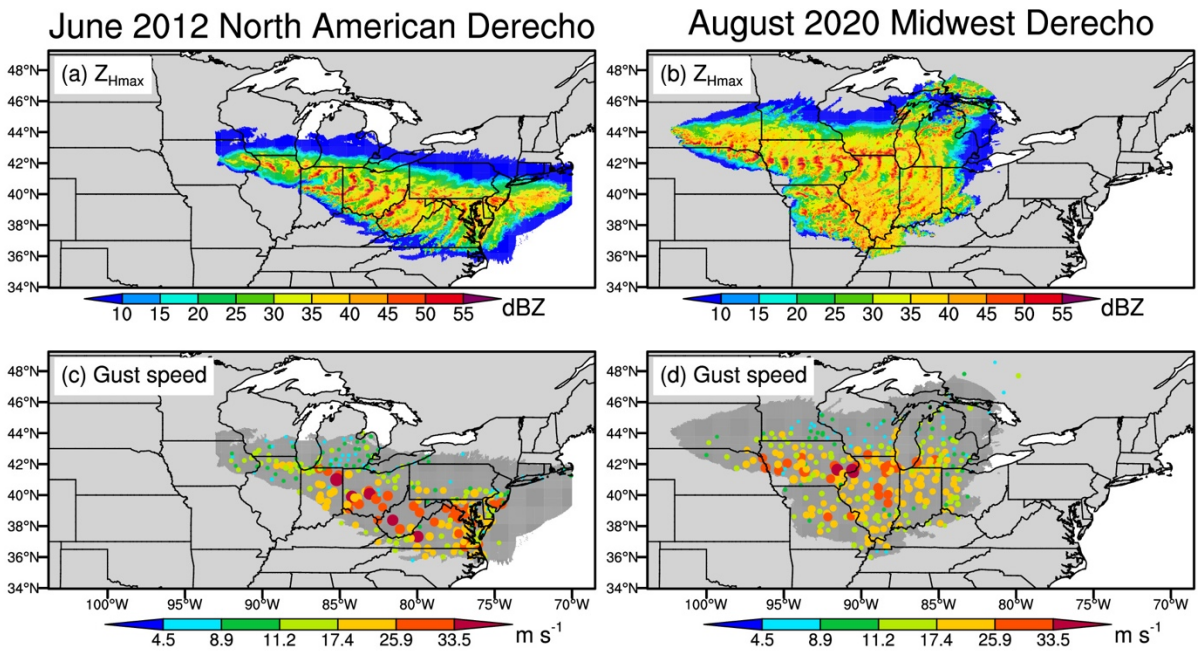

Figure 1. Spatial evolutions of the (a, b) composite (column-maximum) radar reflectivity (Z_{Hmax}) signatures and (c, d) surface gust speeds (colored dots) of two ~~derechos~~DMCSs. The first column is for the DMCS associated with the June 2012 North American derecho, which occurred on 29-30 June 2012, and the right column is ~~for~~ the August 2020 Midwest derecho accompanying DMCS, which occurred on 10-11 August 2020. Due to spatiotemporal overlapping, multiple Z_{Hmax} and gust speeds may exist for a given grid cell or weather station, in which case only the corresponding maximums are shown in the figure. ~~The timings of some bow echo occurrences are labeled in (a) and (b). In (a), "20Z", "21Z", and "22Z" refer to 20:00, 21:00, and 22:00 UTC on 29 June 2012. In (b), "17Z", "18Z", and "19Z" refer to 17:00, 18:00, and 19:00 UTC on 10 August 2020. In (c) and (d), the misty rose shading corresponds to areas with Z_{Hmax} ≥ 40 dBZ, and the dark gray shading refers to derecho coverage with Z_{Hmax} < 40 dBZ.~~In (c) and (d), the dark gray shading refers to DMCS cold cloud coverage. The dot sizes in (c) and (d) are proportional to the gust speed magnitudes. Notably, gust speed in (c) and (d) is based on the hourly maximum gust speed ($gust_{hourly\_max}$), which is the largest gust speed within one hour if multiple gust speed measurements are available.

A reliable derecho dataset is foundational for understanding the underlying physical mechanism of derecho initiation and development and their socioeconomic impacts. Johns and Hirt (1987) developed the first derecho climatology in the warm seasons of 1980-1983 in the United States by quantitatively defining a derecho as a family of downburst clusters produced by an extratropical MCS. Specifically, they required a derecho to satisfy the following six criteria. ~~1)~~

1) There must be a concentrated area of reports with wind damage or convective gusts > 25.7 m s^{-1}, ~~with a~~and the major axis length of the area must be at least 400 km. ~~2) These~~

2) Those wind damage or convective gust reports must show a pattern of chronological progression, either as a singular swath or a series of swaths. ~~3)~~

3) The concentrated area must have at least three reports of either F1 damage (32.7-50.3 m s^{-1}) (Fujita, 1971) or convective gust of at least 33.4 m s^{-1} separated by ≥ 64 km. ~~4)~~

4) At most 3 hours can elapse between successive reports of wind damage or gust > 25.7 m s^{-1}. ~~5)~~

5) The associated convective system must have temporal and spatial continuity in surface pressure and wind fields. ~~6)~~

6) If multiple swaths of wind damage or gust reports > 25.7 m s^{-1} exist, they must be from the same MCS event.

Since then, several other studies have developed derecho climatologies during other periods using slightly different criteria (Bentley and Mote, 1998; Evans and Doswell, 2001; Bentley and Sparks, 2003; Coniglio and Stensrud, 2004; Guastini and Bosart, 2016). For example, Bentley and Mote (1998) removed the third requirement and reduced the elapsed time in the fourth condition from no more than 3 hours to no more than 2 hours in their derecho climatology from 1986 to 1996. In Coniglio and Stensrud (2004), the elapsed time was further changed to no more than 2.5 hours, and the gust reports of at least 33 m s^{-1} were used to separate derechos of different intensities.

Although the aforementioned derecho datasets were generated using different criteria and during different periods (Johns and Hirt, 1987; Bentley and Mote, 1998; Evans and Doswell, 2001; Bentley and Sparks, 2003; Coniglio and Stensrud, 2004; Guastini and Bosart, 2016), they showed many similar derecho climatological characteristics in the United States. For example, derechos occur more frequently in the warm than cold seasons; the Great Plains, Midwest, and Ohio Valley are regions most favorable for derecho development, and few derechos occur in the eastern and western coastal areas. Considering the inconsistent thresholds used in the above studies and the lack of physical mechanisms in their derecho

definitions, Corfidi et al. (2016) proposed a stricter and more physically based derecho definition, which required the existence of sustained bow echoes with mesoscale vortices or rear-inflow jets and a nearly continuous wind damage swath of at least 100 km wide along most of its extent and 650 km long. In addition, the wind damage must occur after the convective system was organized into a cold-pool-driven forward-propagating MCS. Most derechos satisfying this definition would be classified as "progressive" but not "serial." A serial derecho typically originates in strongly forced environments and develops from a mature squall line with multiple embedded bow echoes. In contrast, progressive derechos generally originate from small convective clusters that grow upscale into large organized forward-propagating MCSs in synoptic environments with weak forcing (Squitieri et al., 2023).

It is difficult to develop a derecho climatology using the definition proposed by Corfidi et al. (2016) with current operational measurements, as it involves the identification of bow echoes, rear-inflow jets, and cold pools. However, rear-inflow jets and cold pools are generally associated with bow echoes (Weisman, 1993; Adams-Selin and Johnson, 2010). Once long-lived bow echoes are found in an MCS ~~event~~, we can expect the simultaneous existence of rear-inflow jets and cold pools. Nevertheless, identifying bow echoes, a feature typically identified visually from radar observations, is still challenging for large volumes of data, such as the 30+ year National Oceanic and Atmospheric Administration (NOAA) Next Generation Weather Radar (NEXRAD) archive~~.~~ consisting of 159 radars. The manual examination is time-consuming and sensitive to subjective biases. This study applies a semantic segmentation convolutional neural network (CNN) to detect bow echoes automatically from two-dimensional composite (column-maximum) reflectivity (Z_{Hmax}) data in the United States, which are then combined with an MCS tracking dataset and ~~gust speed measurements from surface meteorological stations~~surface gust speeds to identify derechos using criteria adjusted from Corfidi et al. (2016). After manual examination and validation, we produce a high-resolution (4 km and hourly) observational derecho and DMCS dataset in the United States east of the Rocky Mountains from 2004 to 2021. The dataset comprises two subsets based on different gust speed data sources: one uses gust speed

measurements from the global hourly Integrated Surface Database (ISD) (NOAA/NCEI, 2001), and the other exploits gust speed reports from the NOAA's Storm Events Database (SED). As the first derecho climatology that utilizes a machine learning technique following physically based criteria and covers the recent decades, the dataset provides a reference for future derecho studies and can be used to investigate the underlying mechanisms for derecho initiation and development, the climatological impacts of derechos on hazardous weather, and the damage of derechos to infrastructure and human property.

The remainder of the paper is organized as follows. Section 2 introduces the MCS ~~dataset~~ and gust speed ~~measurements~~datasets used to generate the derecho dataset. Section 3 describes the machine learning (i.e., semantic segmentation CNN) methodology to detect bow echoes, including sampling, training, and evaluation. Section 4 explains our derecho identification criteria in detail. Section 5 evaluates our derecho dataset ~~against~~through cross-validation of the two subsets (ISD-based vs. SED-based) and compare them with previous derecho estimations and the observational data from the NOAA Storm Prediction Center (SPC) in 2004 and 2005. Section 6 analyzes the derecho climatological characteristics. Section 7 shows how to access our derecho dataset, and the study is summarized in Section 8.

2 Source datasets

2.1 MCS dataset

Since previous MCS datasets only cover the period from 2004 to 2017 (Li et al., 2021; Feng et al., 2019), we use an updated version of the Python FLEXible Object TRacKeR (PyFLEXTRKR) software (Feng et al., 2023), which exploits collocated radar signatures, satellite infrared brightness temperature, and precipitation to identify robust MCS events (Feng et al., 2019), to produce an updated 4-km and hourly MCS dataset in the United States east of the Rocky Mountains from 2004 to 2021~~.~~ (Feng, 2024). Several hourly source datasets are used in the generation of the MCS dataset, including the National

Centers for Environmental Prediction (NCEP)/the Climate Prediction Center (CPP) L3 4 km Global Merged IR V1 brightness temperature dataset (Janowiak et al., 2017), the three-dimensional Gridded NEXRAD Radar (GridRad) dataset (Bowman and Homeyer, 2017), the NCEP Stage IV precipitation dataset (CDIACS/EOL/NCAR/UCAR and CPC/NCEP/NWS/NOAA, 2000), and ~~hourly~~ melting level heights derived from ERA5 (European Centre for Medium-Range Weather Forecasts (ECMWF) Reanalysis v5) (Hersbach et al., 2023). The MCS definition criteria are almost the same as those in Feng et al. (2019), such as cold cloud shield (CCS) area > 60,000 km^2, precipitation feature (PF, which is a continuous convective or stratiform area with surface rain rate > 2 mm h^{-1}) major axis length > 100 km, the existence of 45-dBZ convective echoes, etc., except that the duration requirement is lowered to include those convective systems lasting for just 6 hours. This adjustment allows us to capture slightly shorter-lived MCSs that may produce intense wind gusts but are missed in the previous MCS datasets. Convective and stratiform radar echo classification in PyFLEXTRKR follows the Storm Labeling in 3D (SL3D) algorithm (Starzec et al., 2017), which uses horizontal texture and vertical structure of radar reflectivity from the GridRad product. Notably, the GridRad data are available each month from 2004 to 2017 but only between April and August from 2018 to 2021. Since most derechos occur in the warm season (Ashley and Mote, 2005; Coniglio and Stensrud, 2004), missing the cold months between 2018 and 2021 does not affect our derecho climatological analyses in Section 6. For brevity, we do not mention the missing cold months between 2018 and 2021 in the following sections unless stated otherwise.

2.2 Surface gust speed ~~observations~~datasets

~~Surface~~*2.2.1 ISD gust speed measurements* ~~between 2004 and 2021 are from the Integrated Surface Database (ISD) (NOAA/NCEI, 2001),~~

The ISD is developed by the NOAA National Centers for Environmental Information (NCEI) in collaboration with several other institutions. ISD compiles global hourly and synoptic surface observations from numerous sources (e.g., the Automated Surface Observing System and the Automated

Weather Observing System) into a single common format and data model. Besides internal quality control procedures conducted by the source datasets, ISD applies additional quality control algorithms to process each observation through a series of validity checks, extreme value checks, and internal and external continuity checks (Smith et al., 2011). This study uses ISD gust speed measurements passing all quality control checks (NOAA/NCEI, 2018). Notably, there may be multiple measurements at different times within one hour for some stations. To keep the sampling consistency across different datasets used in the derecho identification, we calculate $gust_{hourly\_max}$, which is the largest gust speed of all available measurements within one hour, for each observational site, unless stated otherwise. A total of 4,260 observational sites provide gust speed measurements between 2004 and 2021 in the study domain, of which 3,954 are over land, and the rest are over the ocean or lakes (Figure S1). We have excluded one observational site (ISD station ID: 726130-14755) in the northeastern United States, which has an unrealistic number of damaging gust measurements (more than 1,000 hours), inconsistent with the surrounding sites. We note that although we only use measurements passing all the available quality control checks, spatial quality control is missing in the ISD (Smith et al., 2011). Figure S2a shows that some sites in the eastern United States have apparently more damaging gust occurrences than their surrounding sites, but the occurrence frequencies are less than those stations around the Rocky Mountains. We do not have enough evidence to exclude them from the study. ~~However, the~~The quality of the ISD gust speed measurements will undoubtedly be a source of uncertainty for our derecho dataset. In addition, only 420 ISD sites have continuous gust measurements from 2004 to 2021, while the rest have gust measurements only during part of the study period. The availability of ISD observational sites is another source of uncertainty when identifying derechos.

2.2.2 SED gust speed reports

The SED is also maintained by the NOAA NCEI and serves as NOAA's official publication documenting storms and other significant weather phenomena that are intense enough to cause

socioeconomic damage (NOAA/NCEI, 2025). The National Weather Service (NWS) compiles storm data from a wide range of sources beyond meteorological weather stations and submits them to NCEI. These sources include, but are not limited to, local and federal law enforcement agencies, government officials, Skywarn spotters, NWS damage surveys, the insurance industry, newspaper clipping services, media reports, private companies, and individuals. While the NWS strives to use the best available information, some data in the SED remain unverified due to time and resource constraints. Consequently, the dataset suffers from inaccuracies, inconsistencies, and gaps (Santos, 2016). For example, Ardon-Dryer et al. (2023) found that half of the "dust storms" recorded in the SED had visibilities larger than 1 km, indicating misclassification, while many actual dust storms with visibilities of ≤ 1 km were missing from the dataset. These issues were attributed in part to the diverse sources contributing to the SED and the lack of systematic verification and consistency checks. Considering these limitations, particularly the fact that many strong (≥ 17.43 m s^{-1}) and damaging gust reports in the SED are estimated rather than measured, the derecho and DMCS dataset developed from SED in this study is published as a supplement to the dataset derived from the ISD.

From the SED, we extract measured and estimated gusts, along with their corresponding locations and timestamps, for the period from 2004 to 2021. The raw SED files are available at https://www.ncei.noaa.gov/pub/data/swdi/stormevents/csvfiles/ (NOAA/NCEI, 2025). If a gust report is recorded as a segment, containing both a start and end location with respective timestamps, we process it as two independent reports: one at the start location and time and another at the end location and time. Although the accuracy of the SED gust speeds is not guaranteed, the database provides significantly more strong and damaging gust reports than the ISD due to its inclusion of estimated gusts from various sources. Approximately 82% of SED gust reports from 2004 to 2021 are estimated, while only 18% are measured. However, it is important to note that not all measured strong or damaging gusts are captured in the SED. Given the distinct limitations of both the ISD and SED datasets, we apply different thresholds

criteria for derecho detection depending on the dataset used. These criteria are described in detail in Section 4.

3 Machine learning identification of bow echoes

A bow echo is a bow-shaped pattern with high reflectivity values on a radar image, but its vague definition makes it hard to identify them extensively and efficiently using traditional methods. Instead, we train a semantic segmentation CNN to identify bow echoes automatically from two-dimensional Z_{Hmax} images by performing pixel-level labeling of the bow echo extent. Compared to the manual examination of radar images, machine learning can save a tremendous amount of time and eliminate subjective bias.

3.1 Bow Echo Samples

3.1.1 Initial manual sampling

Our initial bow echo samples are generated based on the named derechos on Wikipedia (https://en.wikipedia.org/wiki/List_of_derecho_events; last access: 19 March 2023~~). We identify~~), corresponding to 54 ~~named derechos~~accompanying DMCSs in the MCS dataset~~ and~~. We manually label times with apparent bow echoes through visual inspection of hourly Z_{Hmax} associated with the tracked ~~MCSs~~DMCSs. Each positive sample is a 384 × 384-pixel (~1536 km × 1536 km) Z_{Hmax} image centered at the corresponding ~~derecho~~DMCS with a bow echo embedded (Figure 2). The number of bow echo samples varies among different ~~derechos~~DMCSs, and 566 positive samples are obtained in total. 5400 negative samples are also randomly selected from the radar reflectivity dataset.

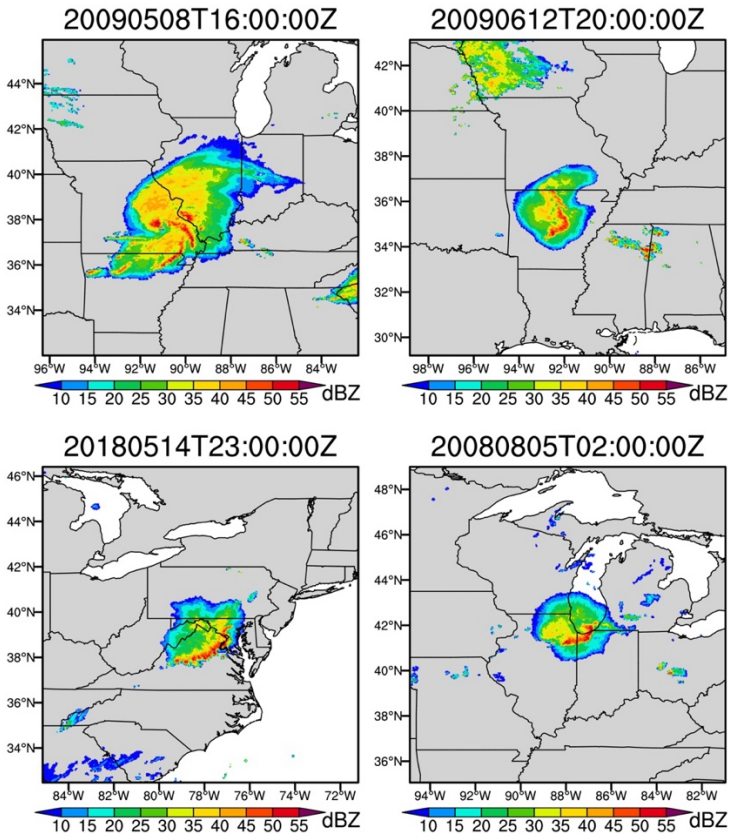

Figure 2. Four examples of bow echoes from the named ~~derechos.~~derecho accompanying DMCSs. The color shading is for Z_{Hmax}. The subplot titles indicate the bow echo timings. For example, 20130613T04:00:00Z represents 4:00 UTC on 13 June 2013.

3.1.2 CNN-based selection of additional bow echo samples

Our initial attempt at developing an automated bow echo detection scheme is to train a classifier CNN — "Dense Net" (Huang et al., 2019) that ingests 384×384-pixel single-channel Z_{Hmax} images and outputs a single classification indicating the presence of a bow echo. Dense Nets are notable for their large number of skip connections~~,~~ (which create multiple paths for data to flow through the network without passing through every layer), and they can achieve comparable performance to very large classifier CNNs with only a fraction of the trainable parameters. Unfortunately, our manual inspection finds that a Dense Net trained on the aforementioned initial samples has a very high false positive rate when applied to the full radar dataset ~~(determined by manual inspection).~~ Although this Dense Net is unsuitable for deployment, the collection of new positive samples it successfully identifies allows us to

supplement the list of known bow echoes and develop a more diverse training set for the following segmentation model.

3.1.3 Pseudo-labeling

By combining the initial samples and the manually selected true positives from the low-quality Dense Net model, we build a semantic segmentation training dataset of 500 unique bow echo snapshots and corresponding hand-drawn bow echo masks. While 500 positive samples are relatively small for a deep learning application, these samples have higher diversity than the initial bow echoes generated from the named derechos on Wikipedia because they are drawn from more distinct events, and, in general, semantic segmentation CNNs can be successfully trained with far fewer samples than image classification CNNs (Bardis et al., 2020).

A relatively low-skill version of the semantic segmentation CNN is trained using the 500 hand-labeled radar images and then applied to the entire Z_{Hmax} dataset. We manually review the bow echo masks produced by this segmentation model and add some of the high-quality masks to a new training dataset. We also collect some of its false positive masks as new negative samples in the new training dataset. This is a semi-supervised learning approach known as "pseudo-labeling" or "bootstrapping" (Van Engelen and Hoos, 2020; Ouali et al., 2020) and is commonly applied to semantic segmentation problems because of the high expense of hand-drawn labels (Peláez-Vegas et al., 2023). The pseudo-labels and hand-labels are combined into a final training dataset with 3677 samples, including 1699 bow echoes and 1978 negative samples, which is used to train the much more skillful semantic segmentation model in Section 3.2.

3.1.4 Data augmentation

To combat the limited training data further, we use several data augmentation strategies when constructing training batches. During training, positive and negative samples are selected with equal

probability, and a batch size of 8 is used. First, random salt and pepper noise is added to 10% of the pixels in each sample with a probability of 0.1. Second, weak random Gaussian noise with a standard deviation of 5 dBZ is added to all the pixels in each sample with a probability of 0.1. Third, samples are flipped in up-down and left-right directions, each with a likelihood of 0.5. Fourth, samples are rotated by 0, 90, 180, or 270 degrees, each with a probability of 0.25. Fifth, samples are randomly shifted vertically and horizontally by -5 to 5 pixels. Sixth, the brightness of the sample image is adjusted by a random factor of -0.6 to +0.2, and the image contrast is randomly adjusted by -0.2 to 0.2. Seventh, the binary target bow echo masks are multiplied by 0.9, and random noise drawn from a uniform distribution between 0 and 0.1 is added. This is known as "soft labels." Lastly, both positive and negative samples are blended with randomly selected negative samples by taking the pixel-wise maximum reflectivity values of the two samples with a 0.5 likelihood. This last data augmentation is unusual but works well in our application because a) reflectivity features typically occupy only a fraction of the sample area, with most pixels being ~~clear-sky~~echo-free and b) bow echoes are high-reflectivity features. When the last data augmentation is applied to a positive sample, the resulting image will typically still contain a bow echo that matches the target mask well.

3.2 Training of U-Net 3+ CNN

Our final semantic segmentation CNN model (Figure 3) uses the U-Net 3+ architecture (Huang et al., 2020). U-Net 3+ is a modern variant of the U-Net architecture (Ronneberger et al., 2015) and differs from the U-Net primarily in the addition of many more skip connections and its multi-resolution loss, which computes loss on rescaled classification masks generated from feature representations at various model levels.

U-Net models were originally developed for the segmentation of biomedical imagery but have been applied to image segmentation problems in other fields and are broadly useful for any image-to-image mapping tasks where the input and target data are the same (or similar) size and shape and merging multi-

resolution information from the input data is important. U-Net CNNs have been applied to a myriad of problems in the atmospheric sciences, such as segmentation (Galea et al., 2024; Kumler-Bonfanti et al., 2020), super resolution (Geiss and Hardin, 2020; White et al., 2024), physics parameterization (Lagerquist et al., 2021), downscaling (Sha et al., 2020), and weather forecasting (Weyn et al., 2021). Perhaps most closely related to this study is Mounier et al. (2022), who used a U-Net to detect bow echoes in simulated radar reflectivity images from a forecast model. A U-Net is an appropriate choice for the segmentation of bow echoes because merging multi-resolution information is crucial for identifying the feature. For example, bow echoes have high reflectivity at the pixel scale, strong reflectivity gradients in the transverse direction at the mid-scale (tens of pixels), and the characteristic bow shape at the large scale (hundreds of pixels).

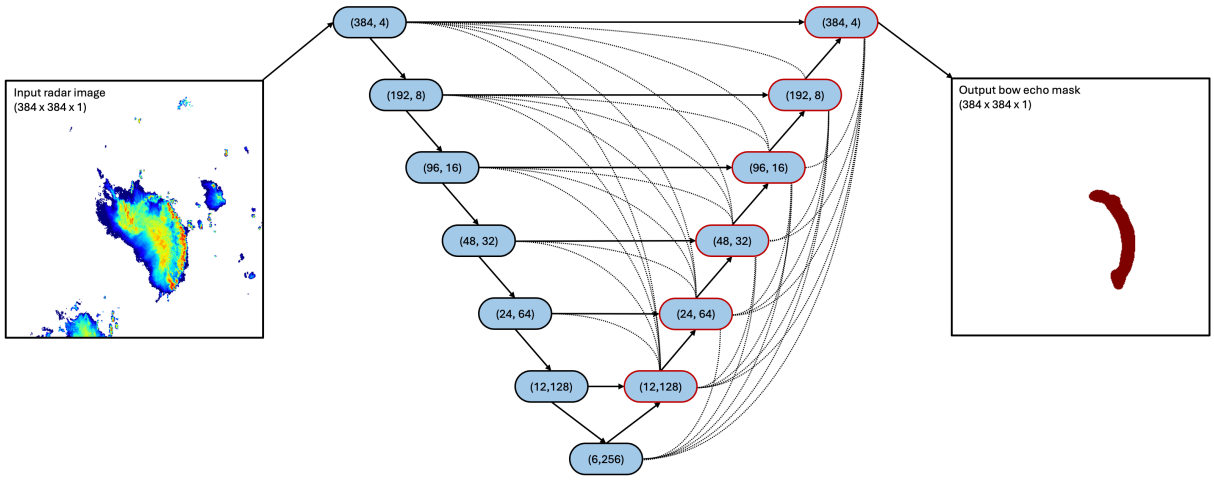

Figure 3. A diagram of our semantic segmentation CNN architecture. The CNN inputs a 384×384-pixel radar image (Z_{Hmax} scaled to 0-255) and outputs a bow echo mask of the same size. The blue ovals represent 3×3 convolutional layers, each followed by a batch normalization layer and a leaky rectified linear unit (ReLU) activation function. The first number in each blue oval indicates the spatial size (for both the width and height) of the output tensor, and the second represents the number of output channels. The solid arrows indicate connections in a standard U-Net architecture, with the downward arrows corresponding to 2×2 max-pooling and the upward arrows corresponding to 2×2 bilinear upsampling operations. The dashed lines represent the skip connections introduced in the U-Net 3+ architecture. These skip connections use max-pooling for spatial downsampling and bilinear interpolation for upsampling, followed by a 16-channel 3×3 convolutional layer with a linear activation. Layers with multiple inputs use channel-wise concatenation to combine those inputs. During training, the output tensors from the layers in the upsampling branch (blue ovals with red boundaries) are scaled to the output spatial resolution and passed through a 1-channel 1×1 convolutional layer with sigmoid activation. Training loss is computed on all 6 of the resulting masks. At inference time, only the mask outputted from the upper-rightmost layer is used.

Our U-Net 3+ CNN ingests 384×384-pixel Z_{Hmax} images where Z_{Hmax} have been clipped to a 0-~~50dBZ~~50 dBZ range and then linearly mapped to a range of 0-255. It is trained using binary cross entropy loss (Bishop, 2006) on masks generated from its 384, 192, 96, 48, 24, and 12-pixel resolution feature representations (Huang et al., 2020), though only the full-resolution (384×384-pixel) output mask is used at inference time. A detailed diagram of the model architecture is shown in Figure 3. Notably, although the model is trained using 384×384-pixel samples, it is a fully convolutional model and can process inputs of variable sizes.

We use the Adam optimizer (Kingma and Ba, 2014) with the Keras default settings (Ketkar, 2017) and an initial learning rate of 0.001 for training. The U-Net 3+ CNN is first trained for 60 epochs composed of 1000 randomly generated training batches of 8 samples each. Then, we decrease the learning rate to 0.0001 and train the CNN for an additional 20 epochs. The training duration is determined by performing an initial 5 rounds of training with 5-fold cross-validation and approximating the epoch numbers to reduce the learning rate and stop training when the mean intersection over union metric plateaus for the validation set. Instead of random shuffling, the validation sets are separated from the training dataset in temporally contiguous chunks to avoid any overlap because, sometimes, multiple samples may be drawn from different times of the same convective system.

3.3 Evaluation of the Semantic Segmentation CNN

We apply the trained U-Net 3+ CNN to the entire Z_{Hmax} dataset and obtain potential bow echo masks over the United States between 2004 and 2021 (Figure 4). As a final post-processing step, we ignore "bow echo" masks with less than 20 pixels (~320 km^2), which are too small to be classified as bow echoes.

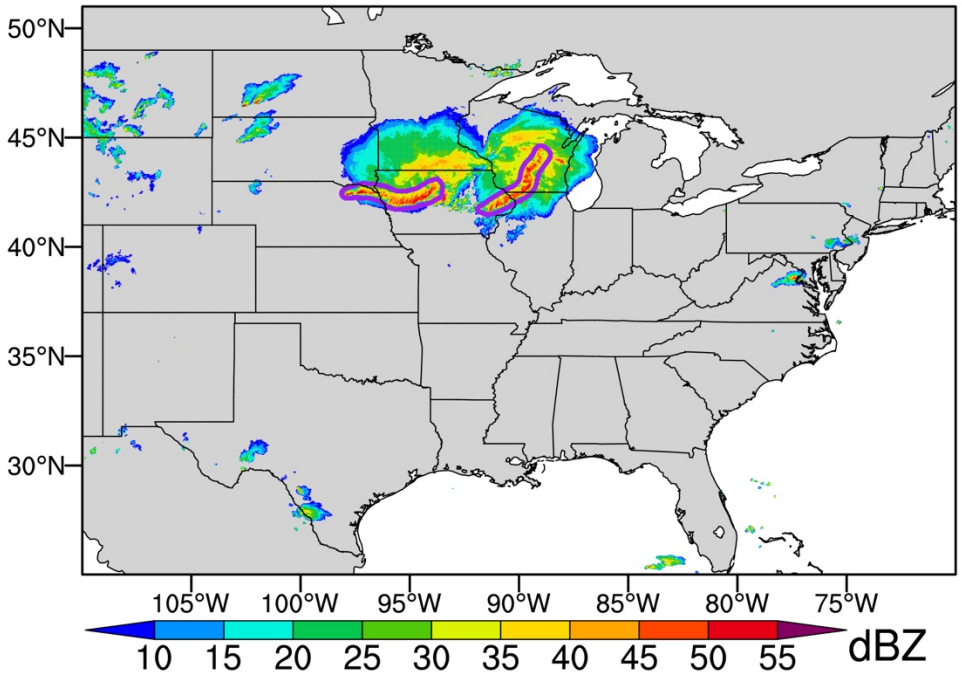

Figure 4. Examples of the U-Net 3+ CNN identified bow echoes (purple contours) based on Z_{Hmax} (color shading) at 5:00 UTC on 17 June 2014.

Instead of validating our segmentation model at a pixel scale, as during the training stage, we prefer evaluating its performance in detecting bulk bow echo features. In other words, we care about whether the segmentation model can recognize the existence of bow echoes and capture their rough locations. Minor spatial biases in bow echo coverage do not affect our below derecho identification much, which contains various flexible criteria to minimize their impacts, such as the buffer zone within 100 km of bow echoes. We also choose to validate the segmentation CNN specifically on MCS events where high reflectivity features are present. Identifying low-reflectivity and ~~clear-sky~~echo-free images as non-bow echoes is desirable for our segmentation model but trivial and not of particular interest for creating a derecho climatology.

To build a testing dataset, we randomly select 217 MCS-associated Z_{Hmax} images in 2010 based on the following requirements. Each image is from a different MCS event. The images have variable sizes and contain the full spatial extents of the MCSs at the selected times; however, they must be at least 192x192 pixels and cannot be drawn from a day that also has a sample in the training dataset. Three of the

authors independently assessed the presence of bow echoes in each image, the results of which are then compared to the segmentation CNN (Table 1). Overall, the CNN model identifies 57 bow echoes, while human labelers 1, 2, and 3 identify 46, 76, and 66, respectively. The average human-human agreement and F_1 scores are 82% and 0.69, while the average human-CNN agreement and F_1 scores are 82% and 0.67 (Table 1). The test indicates that, on the one hand, the detection of bow echoes in radar images is prone to subjective bias; on the other hand, the performance of the segmentation CNN is comparable to that of a human in identifying bow echoes. We emphasize that the CNN bow echo identification is only one component in our following derecho detection criteria, and the adverse impact of this uncertainty is mitigated by other constraints (e.g., almost continuous bow echo existence and strong gusts in proximity with bow echoes).

Table 1 Evaluation of the performance of the segmentation CNN in the bow echo identification[1]

	CNN (57[2])	Person 1 (46)	Person 2 (76)	Person 3 (66)
CNN		84%	79%	83%
Person 1	0.66		77%	88%
Person 2	0.66	0.59		81%
Person 3	0.70	0.77	0.70	

[1]The upper triangular part of the table shows agreement between two independent identifications ($Agreement = \frac{TP+TN}{TP+TN+FP+FN}$), and the lower triangular part shows F_1 scores ($F_1 = \frac{2TP}{2TP+FP+FN}$), which is a better indication of the ability to agree on positives when positives are a minority (Taha and Hanbury, 2015). Here, *TP* denotes true positive, *TN* refers to true negative, *FP* is false positive, and *FN* is false negative. Notably, for the comparison between any two independent identifications, we consider one as "true" and evaluate the other against it (and which set of classifications ~~are~~is considered true does not impact these two metrics).

[2]The number of identified bow echoes from the 217 images.

We match the segmentation CNN detected bow echoes with MCS events from the MCS dataset and identify those MCS-associated bow echoes, which are used to identify derechos in the following section. Figure 5 shows the spatial distribution of MCS-associated bow echo occurrences from 2004 to 2021, which is similar to the MCS spatial distribution with more frequent occurrences in the Great Plains (Li et al., 2021).

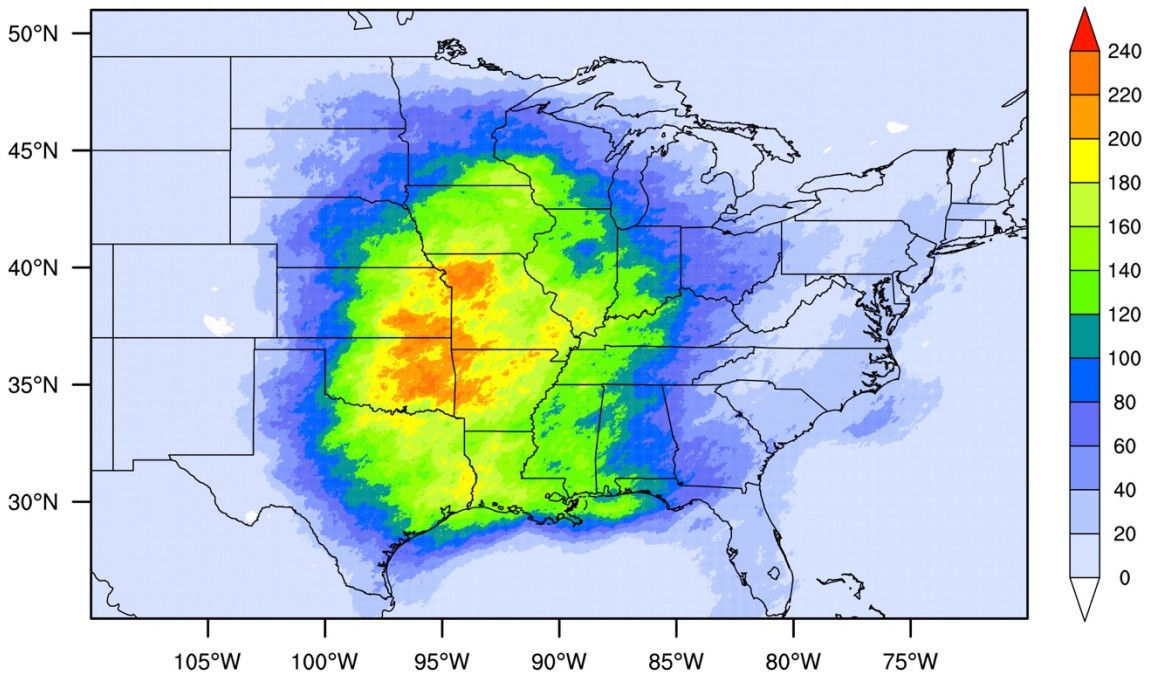

Figure 5. Spatial distribution of the number of MCS-associated bow echoes from 2004 to 2021. Here, we use bow echo masks produced by the segmentation CNN and exclude bow echoes that do not overlap with MCS events. ~~Notably, the PyFELXTRKR-generated MCS dataset contains tropical cyclones (TCs).~~ This figure excludes bow echoes from those non-derecho ~~MCS events~~-producing MCSs that overlap with tropical cyclones (TCs) from the International Best Track Archive for Climate Stewardship (IBTrACS) Version 4 data over the North Atlantic basin (Knapp et al., 2010) following the approach of ~~(~~Feng et al.~~,~~. (2021).

4 Derecho identification

4.1 Derecho definition

As mentioned above, we adopt the derecho definition proposed by Corfidi et al. (2016) but revise ~~some~~certain criteria based on previous studies (Johns and Hirt, 1987; Bentley and Mote, 1998) and ~~the limitation of the observational datasets used in this study so that they can be used in the~~dataset limitations to facilitate objective identification of derechos. Our ~~detailed definition~~final criteria are summarized below~~.~~, with detailed explanations provided afterward (Figure 6).

1) A derecho must be attached to an MCS from the MCS dataset.

2) The derecho must persist for at least 5 hours, with a bow echo present for at least 80% of its lifetime. In addition, gaps between successive bow echo occurrences cannot exceed two hours.

All bow echoes must belong to the same bow echo series, as defined in the subsequent explanation.

3) The derecho bow echo series must exhibit forward propagation, based on two modified criteria from Corfidi et al. (2016):

- The acute angle between the averaged bow echo orientation and the bow echo series' propagation direction must exceed 45° (Figure 6).
- The propagation speed of the bow echo series must be at least 30% greater than the background mean wind speed at 500 hPa, derived from ERA5 data. The methodology for calculating the averaged bow echo orientation, bow echo series' propagation direction and speed, and the background mean wind speed is detailed in Appendix A.

4) Derecho-associated gust speed criteria vary based on the gust speed source dataset:

- For ISD data: Within 100 km of the derecho-accompanied bow echoes (termed the "derecho area"), there must be at least 10 sites with strong gusts (≥ 17.43 m s^{-1}) and at least 1 site with damaging gusts (≥ 25.93 m s^{-1}).
- For SED data: At least 10 locations must report damaging gusts.
- The fraction of sites with strong/damaging gusts (ISD) or damaging gusts (SED) must be ≥ 20%.
- Gaps between successive strong (ISD) or damaging (SED) gust reports cannot exceed two hours.
- The gust swath must be at least 650 km in length and 100 km in width. Swath length and width calculations are explained below.

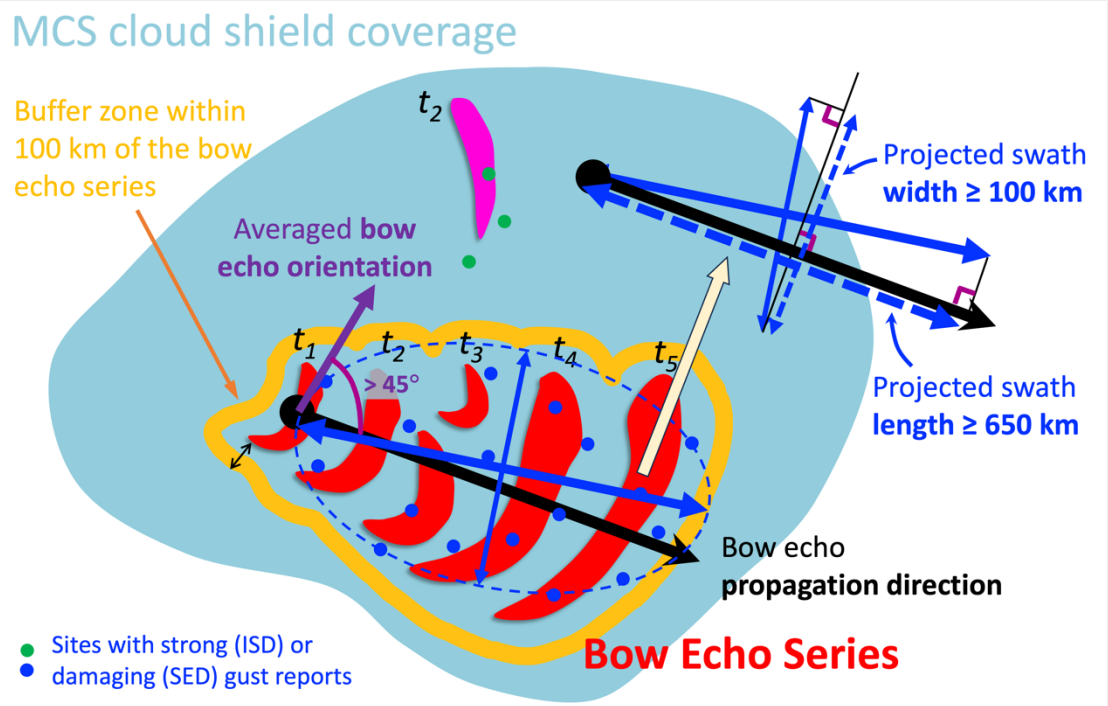

Figure 6. Schematic of the automated detection algorithm. Red and pink objects represent bow echoes. At time t_2, there are two bow echoes belonging to different bow echo series due to their great distance from each other. In contrast, the two bow echoes at t_3 are from the same bow echo series since they are close to each other. The pink bow echo at t_2 is far from the bow echoes at t_1 and t_3. Therefore, they belong to different bow echo series. The sites (green dots) with strong (for ISD) or damaging (for SED) gusts outside the 100-km buffer zone of the bow echo series (i.e., the derecho area) are excluded from the strong (ISD) or damaging (SED) gust swath calculation. The black arrow indicates the propagation direction of the bow echo series, and the violet arrow indicates the averaged bow echo orientation. Their acute angle must be > 45° for a derecho. The upper-right corner illustrates how the major and minor axis lengths of the gust fitted ellipse are projected onto another coordinate paralleling to the bow echo series' propagation direction to calculate gust swath length and width.

4.2 Explanation of Key Criteria and Adjustments

Criterion 1: MCS Association

~~1)~~ This is ~~the most~~a straightforward requirement and ~~one~~a major advantage of our ~~advantages~~approach. Due to the lack of a reliable MCS dataset, ~~most~~ previous studies often spent ~~much~~considerable effort identifying spatiotemporally continuously propagating convective systems (Squitieri et al., 2023).

~~2) At least one derecho feature (DF) exists in the MCS lifetime. A DF is defined as a continuous period satisfying the following criteria (Figure 6).~~

Criterion 2~~.1) The DF must last for at least 2 hours,~~: Bow Echo Occurrence and Series Definition

The 80% bow echo ~~occurs during ≥ 80% of the DF period. For example, if the DF lasts for 10 hours, it must have bow echoes in at least 8 hours. In addition, no more than 2 hours can elapse between successive bow echo occurrences. In other words, bow echo must exist for at least one~~ occurrence threshold and the ≤ 2-hour ~~in any two~~ lapse time between consecutive ~~hours. The above two thresholds consider the~~ bow echoes account for uncertainties in the segmentation CNN identification ~~uncertainty~~process and the diversity of MCS events. ~~Moreover, a DF requires these bow echoes to be from the same~~

A bow echo series~~.~~ is defined in two steps:

1. Spatial grouping: Within a given MCS, bow echoes occurring in the same hour are categorized into separate series if they are more than 100 km apart.
2. Temporal linking: Successive bow echoes (no more than 2 hours can elapse between their occurrences) are considered part of the same series if they are less than 200 km apart, even if they were initially classified as separate series.

Due to merging or splitting or the complex nature of some convective systems, a bow echo at one hour may be far from the bow echoes right after or before that hour or another bow echo during that hour (Figure 6). In such a rare situation, these bow echoes are unlikely caused by the same physical process and, therefore, do not belong to the same bow echo series~~. We separate different bow echo series in two steps. First, a distance criterion categorizes multiple bow echoes in the same hour into different series. Any bow echoes more than 100 km from each other belong to different series. Second, we temporally connect bow echoes from the same series using another distance threshold. The distance between two~~

~~successive bow echoes (no more than 2 hours can elapse between their occurrences) from the same series must be no more than 200 km. Notably, the second step can overwrite the first step. For example, two bow echoes at hour t belong to different series in the first step, but in the second step, they are close enough (≤ 200 km) to the same bow echo at hour t–1. If so, they are considered from the same bow echo series~~ (Figure 6). The above stepwise approach ensures that bow echoes from different physical processes are not incorrectly grouped.

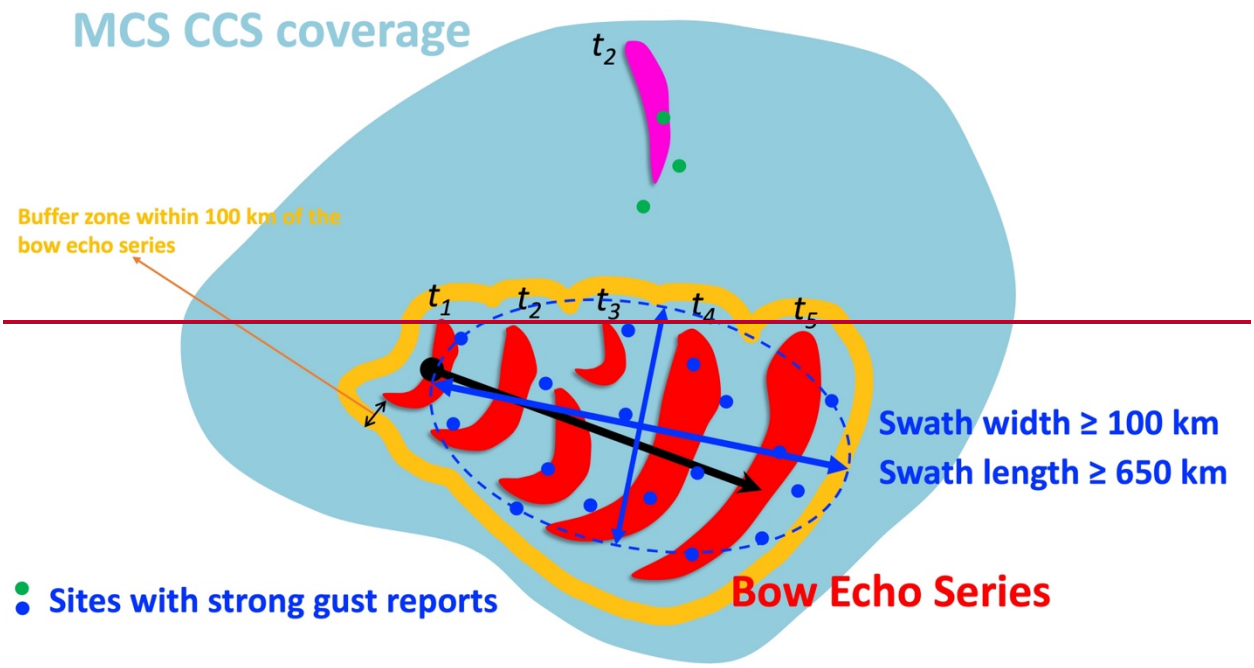

~~Figure 6. Schematic of the automated detection algorithm. Red and pink contours represent bow echoes. At time t_2, there are two bow echoes belonging to different bow echo series due to their great distance from each other. In contrast, the two bow echoes at t_3 are from the same bow echo series since they are close to each other. The pink bow echo at t_2 is far from the bow echoes at t_1 and t_3. Therefore, they belong to different bow echo series. The sites (green dots) with strong gust reports outside~~Criterion 3: Forward Propagation Adjustment

We modify the ~~100-km buffer zone~~Corfidi et al. (2016) criterion of "nearly orthogonal" to > 45° for the acute angle between the averaged bow echo ~~series (i.e., the DF area) are excluded from the strong gust~~

~~swath calculation. The black arrow indicates~~orientation and the bow echo series' propagation direction. This adjustment:

- Accounts for segmentation CNN uncertainties, particularly in the propagation direction ~~of the bow echo series~~estimation.
- ~~2.2) We calculate the DF-associated maximum gust speed for each land observational site during the DF period. Within 100 km of the DF bow echoes, which we name the DF area, there must be ≥ 10 sites with strong gusts (gust speed ≥ 17.43 m s^{-1}) and ≥ 1 site with damaging gusts (gust speed ≥ 25.93 m s^{-1}). In addition, the~~ Reduces false exclusions caused by minor variations in orientation.

Criterion 4: Gust Speed and Swath Calculation

The 20% fraction ~~of sites with strong gusts should be ≥ 20%. This fraction criterion is intended~~threshold is introduced to exclude ~~potential~~ MCSs potentially associated with extratropical cyclones, which ~~could~~often produce isolated strong or damaging gusts ~~over limited observational sites~~ but weaker gusts ~~at~~across most ~~other sites. Besides, a DF requires that no more than 2 hours can elapse between successive strong gust reports. Then, we calculate the major and minor axis lengths of the fitted~~sites.

To determine the gust swath length and width:

1. We fit an ellipse ~~swath using the locations of those~~around sites with strong ~~gust reports~~(ISD) or damaging (SED) gusts in the derecho area (Figure 6). ~~As a DF,~~
2. Since the ellipse may not align with the bow echo series' propagation direction, we project its major and minor axes onto a new coordinate system based on the bow echo propagation direction, as shown on the upper right corner of Figure 6. The projected major or minor axis length that is parallel to the bow echo propagation direction is the gust swath length, and the

projected minor or major axis ~~lengths must be at least~~length that is perpendicular to the propagation direction is the swath width. Notably, both major and minor axis lengths can be projected parallelly and perpendicularly. If major axis length is projected parallelly, the minor axis length must be projected perpendicularly, and vice versa. Thus, we obtain two pairs of swath length and width.

3. We consider the uncertainties of the bow echo propagation direction when conducting the projection. In detail, we conduct projections iteratively by varying the propagation direction values with an interval of 0.2° within ±10° of the initial calculated bow echo series' propagation direction. Therefore, we obtain $\left(\frac{20}{0.2}+1\right)\times 2 = 202$ pairs of swath length and width in total. As long as one pair of swath length and width satisfies length ≥ 650 km and ~~100~~width ≥ 100 km, Criterion 4 is satisfied.

If no derecho is identified for a given MCS using the above definition criteria, we can relax the distance requirement (100 km) in Criterion 4 to be within 200 km of the derecho-associated bow echoes that satisfy the condition that there is no bow echo from the same bow echo series an hour ago or later during the derecho's lifetime. If the bow echo is in the first hour of the derecho's lifetime and there are no bow echoes for the corresponding MCS an hour ago, we can also extend the distance threshold to 200 km. This is similar to the bow echo in the last hour of the derecho's lifecycle but without CNN-identified bow echoes an hour later. Notably, the distance extension is optional. For the bow echoes satisfying the above conditions, the distance threshold can be either 100 or 200 km. Using 100 km is superior to using 200 km until we find a derecho if it exists. The distance extension is also intended to minimize the impacts of the bow echo identification error. If a bow echo is missed in the semantic segmentation procedure, extending the distance threshold can include strong ~~, respectively.~~ and damaging gusts associated with the missed bow echo, thus slightly reducing the derecho detection error.

We emphasize that, in Criterion 4, our ISD gust speed criteria are weaker than the SED gust speed criteria as well as those of previous studies (Squitieri et al., 2023; Bentley and Mote, 1998; Johns and Hirt, 1987), which also estimated the gust swath based on SED damaging gusts. ~~Moreover, previous studies often required a few~~ As mentioned in Section 2.2.2, most SED gust reports ~~of gust speed ≥ 33 m s^{-1}. Notably, many gust speeds in earlier studies were from post-disaster~~are estimates, while ~~this study uses~~ ISD ~~surface station~~ provides gust measurements~~. Post-disaster~~ from weather stations. SED estimates can capture potential damaging gust occurrences over a much larger area~~.~~, although with large uncertainties. In contrast, due to the limited coverage of observational sites, real-time ISD measurements may miss substantial damaging gust occurrences in nearby regions. Therefore, we lower the gust speed criteria to capture potential derechos when using ISD measurements. It does not mean that the ISD-based derechos are weaker than the SED-based ones or even not derechos, as elaborated in Section 5.

~~2.3) If no DF is identified for a given MCS using the above procedures, we can relax the distance requirement in (2.2) to be within 200 km of the DF bow echoes that satisfy the condition that there is no bow echo from the same bow echo series an hour ago or later during the DF period. If the bow echo is in the first hour of the DF period and there are no CNN-identified bow echoes for the MCS event an hour ago, we can also extend the distance threshold to 200 km. This is similar to the bow echo in the last hour of the DF period but without any CNN-identified bow echoes an hour later. Notably, the distance extension is optional. For the bow echoes satisfying the above conditions, the distance threshold can be either 100 or 200 km. Using 100 km is superior to using 200 km until we find a DF if it exists. The distance extension is also intended to minimize the impacts of the bow echo identification error. If a bow echo is missed in the semantic segmentation procedure, extending the distance threshold can include strong gusts associated with the missed bow echo, thus slightly reducing the derecho detection error.~~

~~We identify 537 derechos~~ 4.3 Derecho detection results and postprocessing

Using ISD gust measurements, the objective detection algorithm identifies 245 derechos and associated DMCSs between 2004 and 2021~~ using the above objective detection criteria, with an~~. A notable example ~~of~~is the June 2012 North American derecho ~~shown in~~ (Figure 7~~.~~). Figure 7a displays the CNN-identified bow echoes of the DMCS, and Figure 7b shows the ~~DF~~derecho area and associated gust speeds. As expected, the derecho produced ~~extensive~~widespread strong gusts~~ during its DF period~~.

~~Although we have considered~~To further refine the ~~segmentation CNN bow echo identification uncertainties in the above derecho definition criteria, there is no guarantee that every specific situation is considered. Therefore, we carefully examine all the identified~~ISD dataset, we manually review all detected derechos and ~~remove 32 events that are possibly~~DMCSs, removing 31 false detections ~~primarily~~ due to ~~the false~~erroneous bow echo identification ~~of bow echoes~~ (Figure S3). In addition, we ~~manually~~ examine ~~all~~1099 MCS events~~ (808 in total, excluding the aforementioned 537 automatically identified derechos)~~ that produce extensive strong (≥ 10 observational sites) and damaging (≥ 1) gusts over land areas with a strong and damaging gust swath (fitted ellipse) of at least 650 × 100 km^2~~.~~ (the ellipse's major and minor axis lengths). Our manual examination primarily focuses on bow echo identification errors but ~~does not change any of the above derecho definition~~also slightly lower the forward propagating criteria thresholds ~~or parameters.~~for two potential derechos. For those MCSs ~~(55 events in total)~~ that are potential ~~derechos~~DMCSs based on our visual inspection, we manually label their bow echo occurrences that fail the segmentation identification during potential ~~DF periods~~derecho lifetimes (Figure S4) and rerun the automated derecho detection algorithm. Finally, ~~51 events meet~~60 additional derechos are added, bringing the ~~derecho detection criteria described above.~~final total to 274 ($245 - 31 + 60 = 274$).

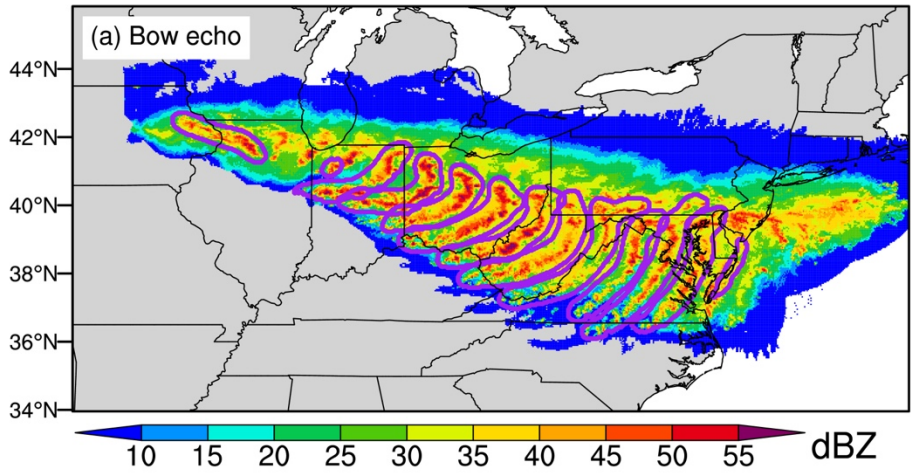

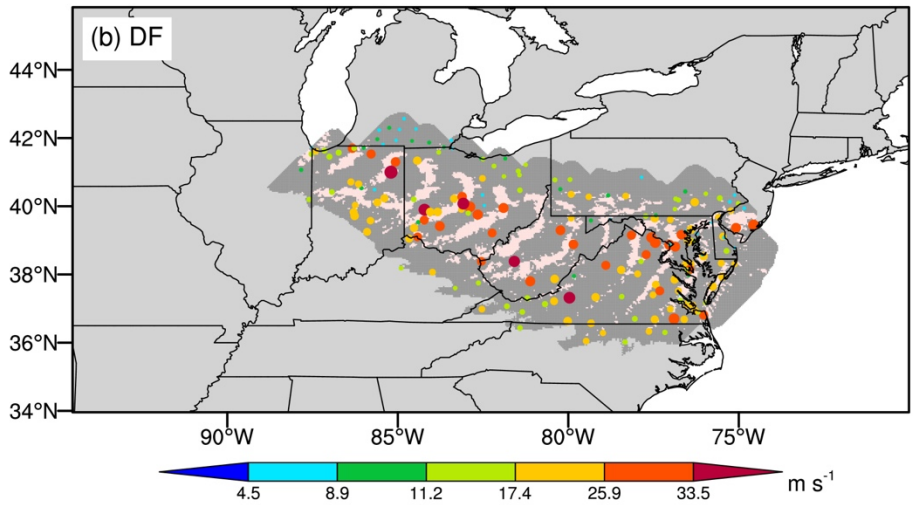

Using the same procedures for SED gust reports, we identify 220 derechos.

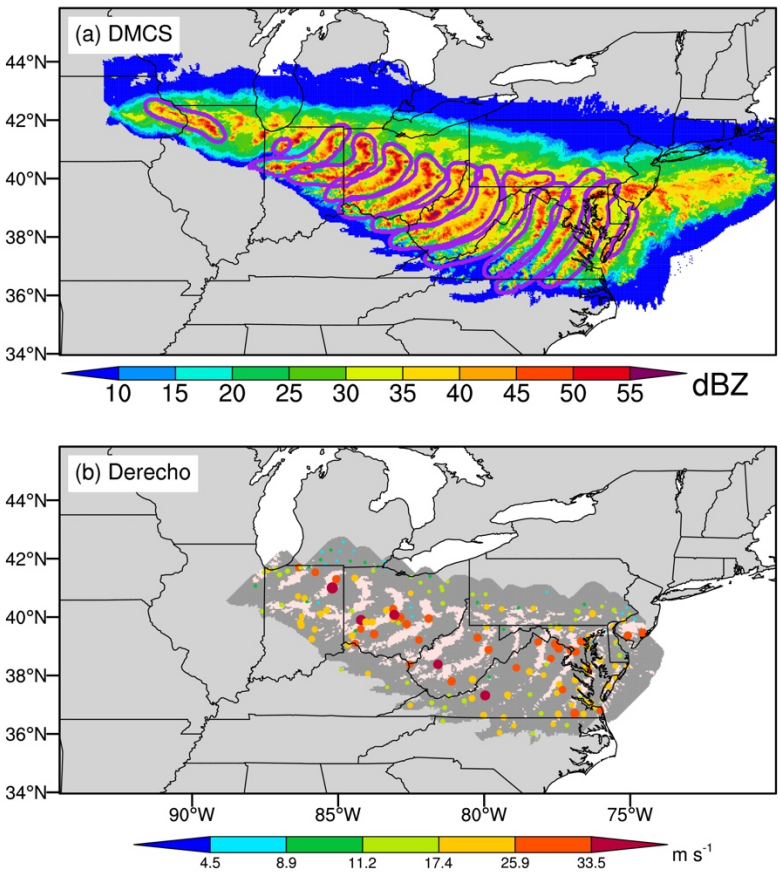

Figure 7. (a) Spatial evolution of Z_{Hmax} (color shading) and CNN-identified bow echoes (purple contours) from the DMCS associated with the June 2012 North American derecho. (b) ~~Spatial evolution of~~Similar to (a) but for the ~~corresponding DF~~derecho period. The ~~DF~~derecho lasted from 17:00 UTC on 29 June to 6:00 UTC on 30 June 2012. The misty rose shading in (b) corresponds to $Z_{Hmax} \geq 40$ dBZ, while the gray shading refers to the ~~DF~~derecho area. Colored dots are the same as those in Figure 1c, except only the ~~DF~~derecho-associated gust measurements are shown.

5 Dataset evaluation and uncertainty

~~Finally, we obtain 556 derechos between~~ 5.1 Evaluation against existing datasets

Between 2004 and 2021, ~~505 of which are identified automatically and 51 of which are added manually. The number of~~our automated detection algorithm identifies 274 derechos (~ 15 per year) using ISD gust measurements and 220 derechos ~~(30.9~~(~12 per year) ~~is much larger than~~using SED gust reports.. These numbers fall within the range of previous estimations (6.1-20.9 per year) ~~using~~based on a ~~major axis~~400 km swath length threshold ~~of 400 km~~ and conventional derecho definitions, as introduced in

Section 1 (Squitieri et al., 2023; Johns and Hirt, 1987; Bentley and Mote, 1998; Evans and Doswell, 2001; Guastini and Bosart, 2016; Ashley and Mote, 2005). ~~The number is also much larger than the result of~~ However, our derecho counts are substantially higher than those reported by Corfidi et al. (2016), ~~which~~who identified only 25 derechos in the warm seasons ~~during~~of 2010-2014 using a ~~major axis~~650 km swath length threshold ~~of 650 km. The large~~. These discrepancies ~~are~~ likely ~~related to our usage of strong gusts but not damaging gusts~~ stem from differences in the methods used to calculate ~~wind damage~~gust swath length and ~~other definition~~width, the criteria~~. However,~~ for forward propagation, and the diverse observational ~~datasets used in the derecho detections also play a critical role. Previous studies did not have an available MCS dataset; as a result, many of their definition criteria were intended to capture MCS events. In contrast, we have developed a high-quality, high-resolution MCS tracking dataset using PyFLEXTKR and many coincident ground-based and remote-sensing observations. Our definition criteria purely focus on the derecho properties and generation mechanism. Previous studies may underestimate~~ source datasets used in the derecho ~~number due to missing MCS events. We confirm this by comparing the derechos from~~ detection.

To further evaluate our dataset, we compare it against the NOAA Storm Prediction Center (SPC ~~with our~~) derecho ~~dataset in~~data from 2004 and 2005 ~~(Table 2). The NOAA SPC data~~ (https://www.spc.noaa.gov/misc/AbtDerechos/annualevents.htm; last access: November 17, 2023~~). provide more~~) (Table 2). This dataset provides detailed timings and locations of derechos ~~in 2004 and 2005 than previous studies (Squitieri et al., 2023), which~~or convective windstorms of near-derecho size, and it is the only available dataset that we can use to evaluate our derecho dataset at the event scale. ~~Notably,~~However, it is important to note that the NOAA SPC data ~~contains~~does not ~~only~~explicitly distinguish between derechos ~~but also~~and convective windstorms of near-derecho size, and ~~we do not know which event is a~~it relies on the conventional derecho ~~or a convective windstorm of near~~ definition, which can significantly influence derecho ~~size. In addition~~counts. Additionally, the NOAA SPC data is

based on SED gust ~~speed measurements and post-disaster estimations. There is not~~reports and lacks an underlying MCS ~~dataset for the NOAA SPC data~~database.

The NOAA SPC ~~data~~dataset contains 50 derechos and near-derecho size convective windstorms ~~of near-derecho size, 22~~for 2004 and 2005, 15 of which are ~~directly captured~~ detected by ~~the automated detection procedure, and 2 of which can be captured after we manually correct the segmentation CNN bow echo identification errors.~~our algorithm using ISD gust measurements. The number increases to 19 when using SED gust reports. Five of the 50 events are entirely ~~missed~~absent in ~~the~~our MCS dataset, possibly because ~~they move too fast and do not meet the PyFLEXTRKR >~~their associated MCSs moved too rapidly to satisfy PyFLEXTRKR's 50% areal overlap ~~tracking~~ criterion using ~~the~~ hourly ~~combined~~ satellite and NEXRAD dataset, or they ~~break~~failed to meet other MCS requirements in PyFLEXTRKR (Feng et al., 2019). ~~We emphasize that 10 of the 50 NOAA SPC events are not derechos based on the actual gust speed measurements since we do not find any land~~ The remaining discrepancies arise from factors such as an insufficient number of damaging gust reports ~~associated with the MCS events. Seven of the 50 events are not derechos using the major axis length threshold of 650 km and the minor axis length threshold of 100 km, even if we consider all the observational sites associated with the events, regardless of whether they are in proximity with the~~ or bow echoes~~. One event is an extratropical cyclone. These 18 events are excluded from derechos using more objective or consistent criteria as NOAA SPC. The remaining three of the 50 events are missed in our derecho dataset due to the criteria used in our~~ , too small a gust swath, or lack of forward propagation. Conversely, our detection algorithm identifies several derechos (4 from ISD and 3 from SED) that are not present in the NOAA SPC dataset. Overall, while most derechos identified by our algorithm are captured in the NOAA SPC data, our derecho counts are notably lower due to our stricter physically-based derecho definition, ~~two of which are due to too few sites with strong gusts, and one is due to the violation of the bow echo and gust speed criteria. In summary, after excluding those 18 non-derechos and the five missed events in the MCS dataset, the~~

~~identification accuracy of our automated~~which reduces the number of events classified as derechos compared to conventional definitions.

Cross validation between the ISD-based and SED-based datasets further supports the robustness of our detection ~~approach is $\frac{22}{50-18-5} = 81\%$ (Table 2). Even if we consider the five missed MCS events, the accuracy can reach up to $\frac{22}{50-18} = 69\%$. For the final derecho dataset with the 51 manually added events, the accuracy is $\frac{22+2}{50-18} = 75\%$. Finally, our derecho dataset identifies 14~~algorithm (Figure 8). A total of 172 derechos are detected by both datasets, while 48 events are identified only in SED and 102 events are unique to ISD. Figure 8 also highlights discrepancies between the two datasets, with more ISD-based than SED-based derechos ~~that are entirely missed by NOAA SPC, confirming the underestimation of~~in 2008, 2010, 2014, 2015, 2019, and 2020, while their counts remain similar in other years. Despite these differences, the two datasets exhibit similar interannual variability, with a temporal correlation coefficient of 0.72. The general agreement between the two datasets support our decision to use different gust speed thresholds for ISD and SED in the detection algorithm. However, the observed discrepancies also underscores the critical role of the source datasets in influencing detection results, highlighting the need for more reliable gust speed observations.

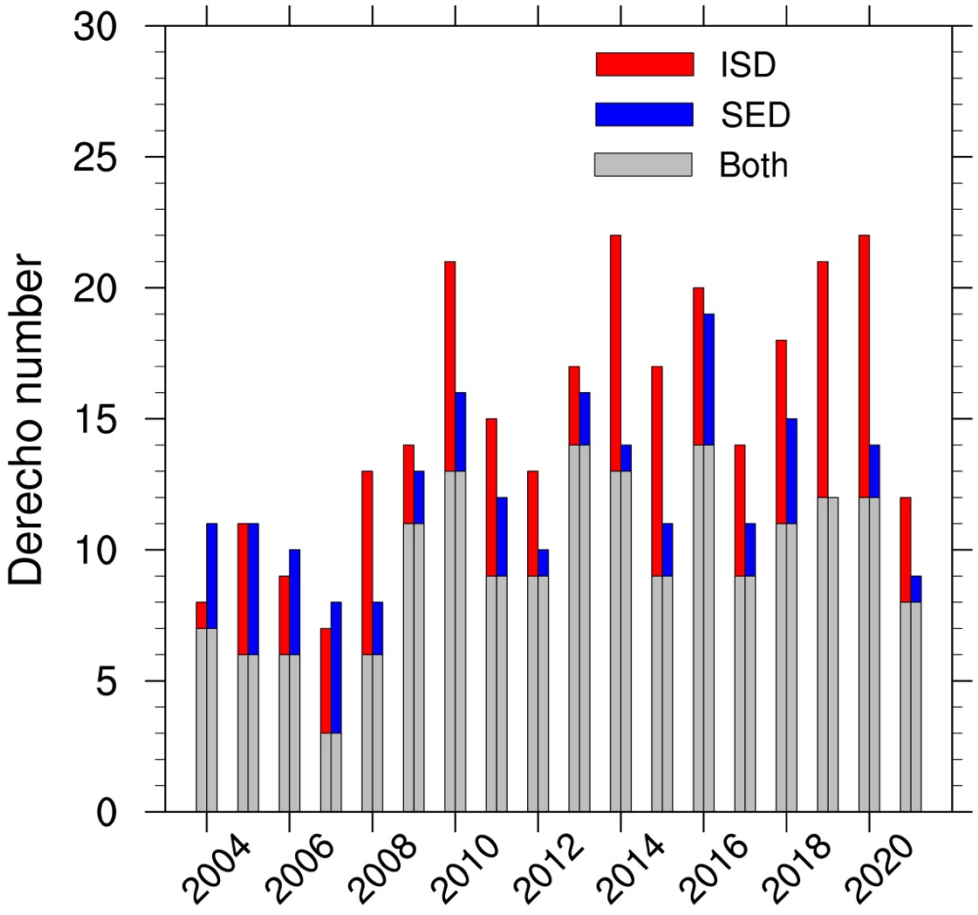

Figure 8. Bar chart of the annual derecho numbers ~~in previous studies due to the lack of a reliable MCS dataset (Squitieri et al., 2023).~~from the ISD-based and the SED-based datasets from 2004 to 2021. Gray shading denotes derechos captured by both datasets, red shading refers to derechos only identified when using ISD gust observations, and blue shading represents SED-only derechos.

Table 2. Evaluation of our derecho dataset against the NOAA SPC data in 2004 and 2005

	Year 2004	Year 2005	Sum
NOAA ~~SPC[1]~~SPC	24	26	50
Captured by ~~our~~the ISD dataset	~~10~~7	~~12~~8	~~22~~15
~~Events missed in~~Captured by the ~~MCS dataset[2]~~SED dataset	~~2~~10	~~3~~9	~~5~~19
~~No land damaging gust, strong gust swath too small, no bow echo, or extratropical cyclone[3]~~	~~10~~	~~8~~	~~18~~
~~Bow echo identification error[4]~~	~~1~~	~~1~~	~~2~~
~~Other criteria~~Derechos in ISD but not ~~satisfied[5]~~in NOAA SPC	1	~~2~~3	~~3~~4
~~Our identified derechos~~Derechos in SED but not ~~listed by~~in NOAA SPC	~~5~~1	~~9~~2	~~14~~3
~~Identification accuracy if excluding those~~NOAA SPC events missed in the MCS ~~events[6]~~dataset	~~83%~~2	~~80%~~3	~~81%~~5
~~Identification accuracy if including those missed MCS events[7]~~	~~71%~~	~~67%~~	~~69%~~

~~[1]NOAA SPC provides the tracks of derechos and other convective systems of near derecho size in 2004 and 2005.~~

~~[2]Some events were moving so fast that the PyFLEXTRKR algorithm, which tracks storms with spatial overlapping > 50%, could not track the systems with the hourly combined satellite and NEXRAD dataset, while some may not meet other MCS criteria.~~

~~[3]Here, "strong gust swath too small" refers to those MCS events with the largest strong gust swath of less than 650 km × 100 km, even if we include those strong gusts not associated with bow echoes.~~

~~[4]It refers to those MCS events with bow echoes not captured by the segmentation CNN. If we manually label the missed bow echoes, they would be identified as derechos.~~

~~[5]It refers to MCS events that do not meet any other criteria (e.g., too few sites with strong gusts) and cannot be classified as derechos.~~

~~[6]$Accuracy = \frac{Captured\ by\ our\ dataset}{Captured\ by\ our\ dataset + Bow\ echo\ identification\ error + Other\ criteria\ not\ satisfied}$~~

~~[7]$Accuracy = \frac{Captured\ by\ our\ dataset}{Captured\ by\ our\ dataset + Bow\ echo\ identification\ error + Other\ criteria\ not\ satisfied + MCS\ events\ missed\ i \square \square\ the\ MCS\ dataset}$~~

~~Although the evaluation against the NOAA SPC data indicates the high quality of our derecho dataset, we must acknowledge its uncertainties caused by several sources.~~

~~The first uncertainty source is~~

5.2 Discussion on dataset uncertainty

Besides the uncertainties in gust speed observations, we acknowledge additional sources of uncertainty affecting our dataset.

5.2.1 Uncertainty from the MCS dataset~~, as mentioned~~

As noted in ~~the~~our evaluation against the NOAA SPC data~~.~~, uncertainties arise from the MCS dataset used in derecho detection. The 50% areal overlap threshold in PyFLEXTRKR, which ~~is set to 50% and used to connect~~links consecutive cold cloud shields (CCSs ~~in the current PyFLEXTRKR configuration, cannot~~), may fail to capture ~~those~~ very fast-moving convective systems ~~with the~~using hourly satellite and NEXRAD ~~datasets. Reducing the~~data. Lowering this threshold ~~will~~would undoubtedly increase the ~~"MCS" and then the "derecho"~~ number of identified MCSs and derechos, but it ~~may~~could also ~~increase the number of~~introduce false tracks that do not belong to the same ~~type of~~ storm system. The 50% threshold ~~of 50%~~ is widely used in ~~the different~~various versions of the FLEXTRKR algorithms (Li et al., 2021; Feng et al., 2023; Feng et al., 2019) and other tracking algorithms based on overlap (e.g., (Whitehall et al., 2015)). ~~Therefore,~~While we ~~would like to keep the overlap~~maintain this threshold ~~as is, but~~in our study, users should ~~realize the~~be aware of uncertainties ~~of the MCS dataset caused by many~~ related to adjustable parameters (e.g., ~~area~~areal overlap threshold, MCS duration, and major axis length) and ~~the~~ limitations ~~of~~in the observational datasets used ~~in~~by PyFLEXTRKR (Feng et al., 2019; Li et al., 2021).

~~The second uncertainty source is related to the segmentation CNN identification of bow echoes. Although the evaluation in Section 3.3 shows the high accuracy of our~~ *5.2.2 Uncertainty from the bow echo identification* ~~and we consider~~

Another key uncertainty arises from the segmentation CNN used to identify bow ~~echo identification uncertainties~~echoes. While our evaluation in ~~the automated derecho detection procedure, we still miss a small fraction of~~ Section 3.3 confirms high accuracy, we acknowledge that some derechos ~~and falsely classify~~may be missed, while some non-derechos may be falsely classified as derechos due to the bow echo identification ~~error. To alleviate the CNN identification~~ errors. To mitigate this issue, we ~~spend much effort manually examining the~~conducted extensive manual verification of derecho and DMCS events ~~identified by the automated algorithm and~~ , as well as other MCS events ~~that produce~~producing widespread strong gusts. However, the manual examination ~~is susceptible to~~ introduces subjective biases, and ~~it is difficult to~~ completely ~~eliminate the~~eliminating bow echo identification uncertainties remains challenging.

~~The third uncertainty source is from the gust speed measurements. Although we only use gust measurements passing the ISD quality control, it is not guaranteed that all gust speeds are reliable and have the same quality, such as the site we exclude in Section 2.2 due to its unrealistic number of damaging gust reports. Moreover, we cannot qualitatively evaluate the impact of the gust measurement uncertainty on the derecho dataset, but users should be aware of the limitations of the gust speed observations.~~

~~The last uncertainty source is related to the~~*5.2.3 Uncertainty from derecho definition criteria*~~. Many~~

Our detection algorithm relies on several adjustable parameters and ~~procedures are used in our algorithm to detect~~ methodological choices, all of which influence the number of identified derechos. ~~There is no doubt that changing these parameters will alter the identified derecho number.~~ For example, if

we ~~change the major axis length threshold of the strong~~require at least three very damaging gust ~~swath to 400 km~~reports (≥ 33.53 m s^{-1}) when using SED, the derecho ~~number will increase to 654 (a 29.5% increase).~~count decreases from 220 to 149. As the first climatological derecho dataset ~~that utilizes~~to incorporate bow echoes ~~in the derecho identification and provides~~and provide detailed event tracking ~~for each event, evaluating the uncertainties of the~~ , a full uncertainty assessment of all tunable parameters is ~~unfeasible and not our priority either.~~beyond the scope of this study. However, ~~based on~~ our sensitivity tests~~, the derecho spatial distribution and seasonal variation patterns in Section 6 generally stay mostly the same with different~~ indicate that changes to key parameters (e.g., reducing the strong gust fraction threshold to 10% or the ~~threshold of the~~ number of sites with strong gust reports to 5~~). The exception is that when we calculate the gust swath length and width using sites (requiring ≥ 10 sites) with damaging gusts as in previous studies (Squitieri et al., 2023), the derecho number is significantly reduced to 19, highlighting the spatial limitation of ISD gust measurements. We emphasize that~~) do not substantially alter the derecho spatial distribution or seasonal variation patterns (see Section 6). Furthermore, our dataset is designed to be flexible: we store all key parameters, allowing users to apply stricter thresholds if needed to focus on stronger derechos.

In summary, although our automated detection algorithm employs a physical-based derecho definition ~~follows Corfidi et al. (2016), we exclude the "forward propagating" criterion they proposed. We try several methods to calculate the angles~~rather than conventional definitions, our derecho counts are comparable to or slightly lower than previous estimations, which is expected given our stricter criteria. Cross-validation between ~~the derecho orientations and their propagation directions but cannot obtain satisfying and accurate results for some events with complex structures. Figure 8 shows the probability density function (PDF) of the angles between "derecho propagation directions" and "bow echo orientations" for all derechos from the final derecho dataset. Based on this type of calculation, 78% of derechos have an angle ≥ 30°, and 58% of derechos have an angle ≥ 45°. For those derechos with angles < 30°, it does not mean that they are not forward propagating systems, but it is more likely that this type of~~

~~angle calculation does not reflect their actual propagation direction. In total, even though we do not use the "forward propagating" criterion in the derecho definition, most of the identified derechos are indeed forward propagating systems~~ISD-based and SED-based datasets supports the high quality of our derecho dataset and the reliability of our detection algorithm. However, users should be aware of the various sources of uncertainty in the dataset generation, particularly those related to gust speed observations, MCS tracking criteria, bow echo identification, and the choice of derecho definition parameters.

~~Finally, users should acknowledge the high quality of our derecho dataset but understand its limitations due to various uncertainties during its generation.~~

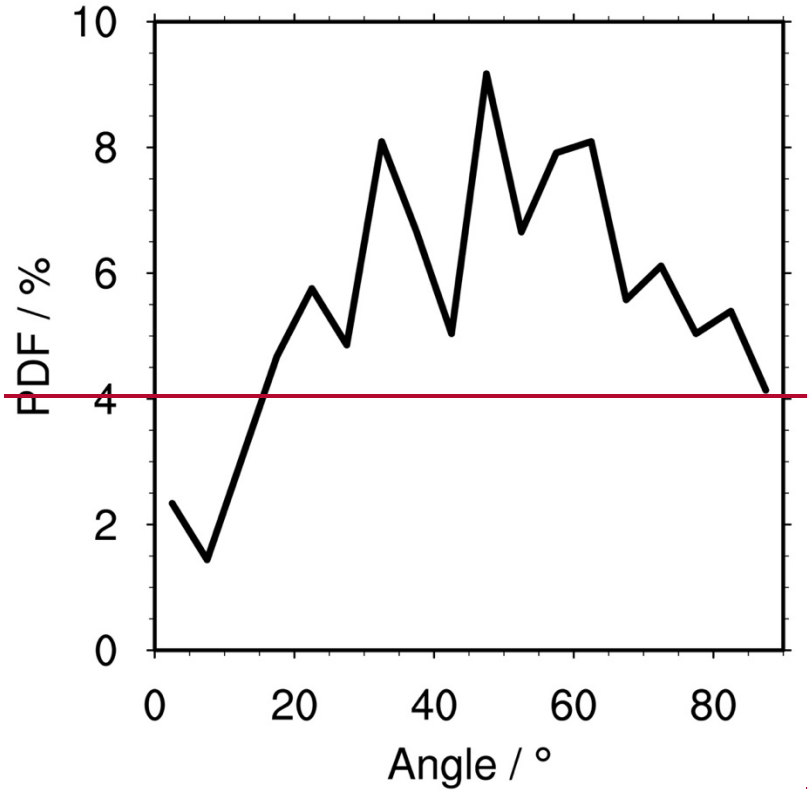

~~Figure 8. The probability density function (PDF) of the angles between derecho propagation directions and bow echo orientations. For any derecho, we calculate all the bow echoes' orientations during its DF period and use the median orientation in the angle calculation. Propagation direction is also based on bow echoes during the DF period. We select any two distinct bow echoes during the period and use their centroid points to derive a direction. If there are n bow echoes, we can obtain $C_n^2 = \frac{n \times (n-1)}{2}$ directions. Similarly, we use the median direction as the derecho's propagation direction to calculate the angle. The angle is initially in the range of -180° to 180°, and we adjust them to be between 0° and 90° to reflect the minimum angle between the derecho's orientation and propagation direction.~~

6 Derecho climatological characteristics

We primarily use the ~~final~~ISD-based derecho dataset ~~with 556 derechos~~ to conduct the following climatological analyses, unless stated otherwise.

6.1 Annual statistics

Figure ~~9~~8 displays the annual derecho numbers from 2004 to 2021. There is an apparent jump in the derecho number before (~~2~~010 derechos per year) and after 2007 (~~3~~015 derechos per year), which may be partially related to the general increase in the number of gust speed observational sites from 2004 to 2010 (Figure S5). Figure ~~10~~9 shows the spatial distribution of yearly averaged annual ISD-based derecho numbers between 2004 and 2021~~, and the derecho paths during their DF periods are displayed in Figure S6~~. The central Great Plains has the most frequent derecho occurrences, extending to Oklahoma in the south, Iowa in the north, Kansas in the west, and Illinois in the east. The areas with frequent derecho occurrences are generally consistent with previous studies (Coniglio and Stensrud, 2004; Guastini and Bosart, 2016; Johns and Hirt, 1987; Ashley and Mote, 2005), although some differences are identified. For example, several studies identified a remarkable northwest-southeast axis with frequent derecho occurrences extending from southern Minnesota to Ohio, which is observable but not apparent in our spatial distribution (Johns and Hirt, 1987; Coniglio and Stensrud, 2004; Guastini and Bosart, 2016). The differences can be caused by many factors, such as distinct derecho definitions and observational datasets used in these studies. ~~We make a sensitivity test by calculating the gust swath using ≥ 10 sites with damaging gusts as mentioned in Section 5, which identifies 19 derechos. The corresponding spatial distribution in Figure S7 well captures the aforementioned west-east axis, although the occurrence frequency is much smaller than in previous studies with more than one derecho occurrence per year (Johns and Hirt, 1987; Coniglio and Stensrud, 2004; Guastini and Bosart, 2016). The sensitivity test seems to indicate that the most intense derechos prefer to occur in the northern Great Plains and Midwest,~~

~~while weaker derechos occur preferably in central Great Plains around the junction of Oklahoma, Kansas, Missouri, and Arkansas.~~When we use SED gust reports in derecho detection, the spatial distribution of derecho counts shows a more noticeable northwest-southeast axis but with lower derecho numbers than the ISD-based dataset (Figure S6).

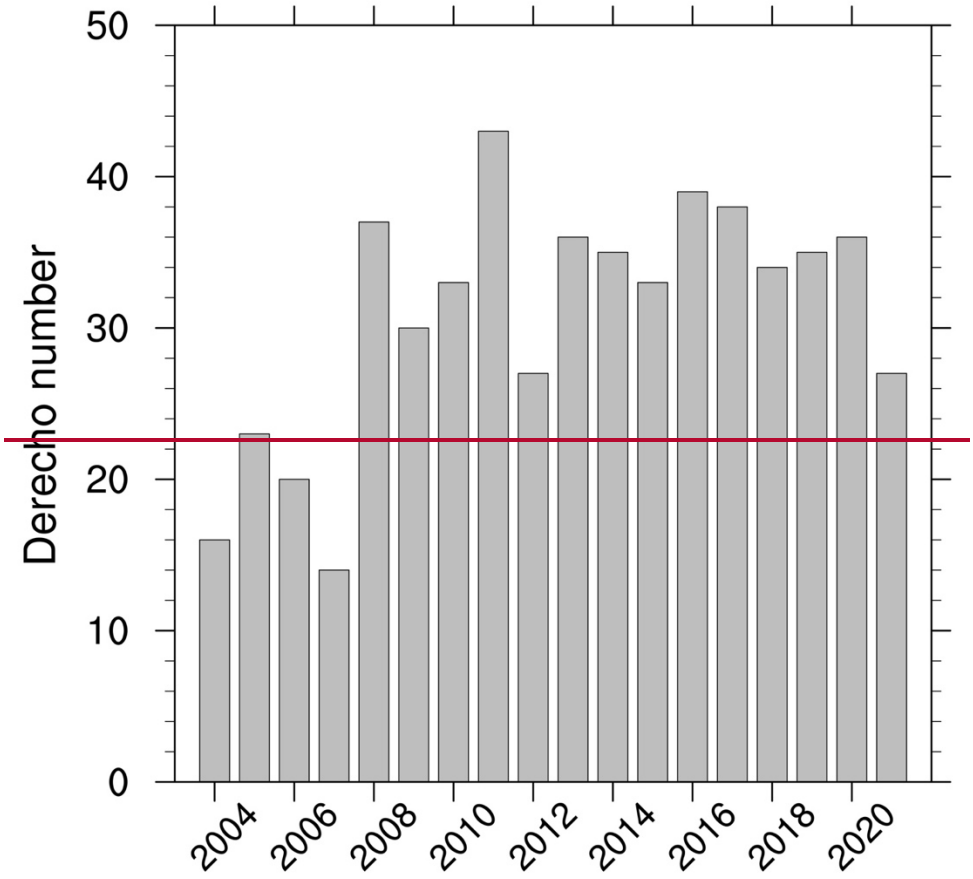

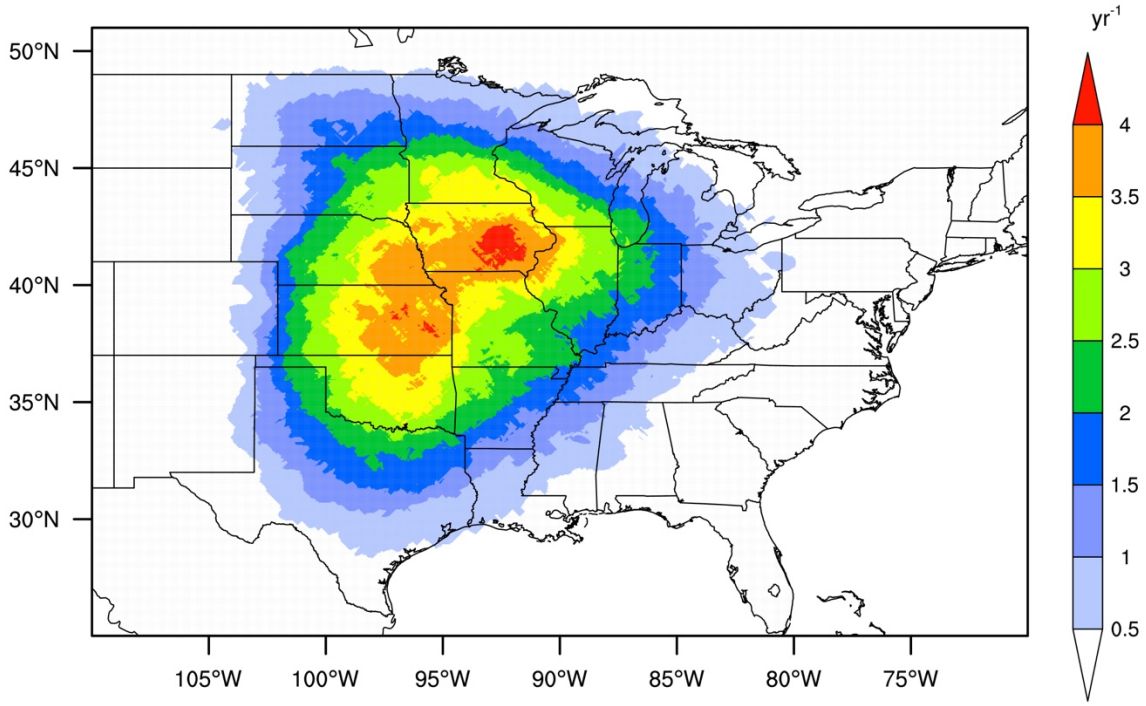

Figure 9. ~~Bar chart of the annual derecho numbers from 2004 to 2021.~~

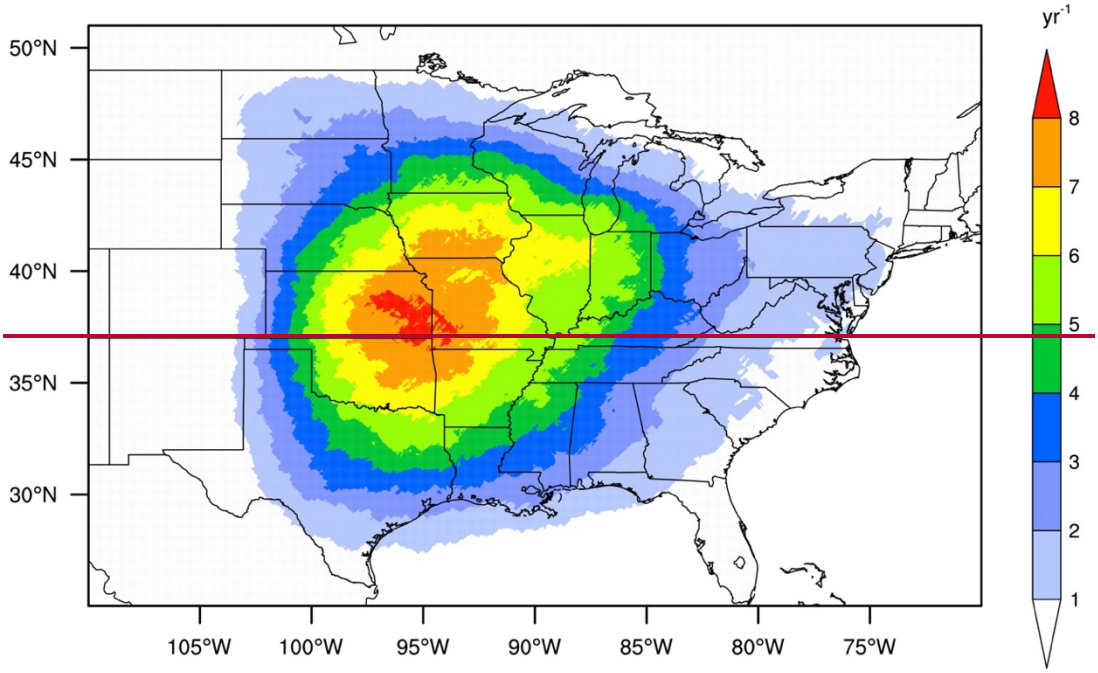

~~Figure 10.~~ Spatial distribution of yearly averaged annual derecho numbers (ISD-based) over the United States east of the Rocky Mountains between 2004 and 2021. Here, we use derecho ~~DF~~ areas as derecho spatial coverages.

6.2 Monthly statistics

Figure ~~11~~10 displays the yearly averaged seasonal variations in the derecho ~~number~~count, with remarkably more derechos in the warm than cold seasons, a feature consistent between ISD- and SED-based datasets and widely captured by previous studies (Ashley and Mote, 2005; Squitieri et al., 2023; Bentley and Sparks, 2003). ~~The derecho seasonal variation resembles that of the MCS events (Feng et al., 2019), similar to the derecho annual spatial distribution (Figure 10 and Feng et al. (2019)).~~However, our dataset has almost no derechos in the code season, which is generally not the case in previous studies. We attribute the difference to our usage of a physically-based derecho definition, which excludes many externally forced convective systems (e.g., extratropical cyclones), which are considered serial derechos in previous studies.

Figure ~~12~~11 shows the spatial distributions of the ~~yearly averaged~~ monthly-mean derecho ~~numbers~~counts based on ISD between 2004 and 2021. On the one hand, many more derechos occur in the warm than cold months. On the other hand, we find remarkable shifts in the areas with the most frequent derecho occurrences from April to August. The region with the most derechos moves northward during the warm season ~~but shrinks zonally.~~. The northward shifts ~~also~~ resemble the MCS events (Li et al., 2021). We can identify two axes with frequent derecho occurrences. One is in the south-north direction along the Great Plains~~,~~ (e.g., June), and the other is in the west-east direction along the northern Great Plains and Midwest~~, which are consistent with the derecho paths in Figure S6.~~ (e.g., July). The axes may represent the two types (serial and progressive) of derechos mentioned in Squitieri et al. (2023). A follow-up study will be conducted to investigate the large-scale environmental conditions associated with different types of derechos based on the developed derecho dataset. ~~Notably, derechos are concentrated in the Lower Mississippi Valley in the cold season, which is also consistent with previous studies (Squitieri et al., 2023~~The SED-based dataset shows similar features but with much fewer derechos in June (Figure S7).

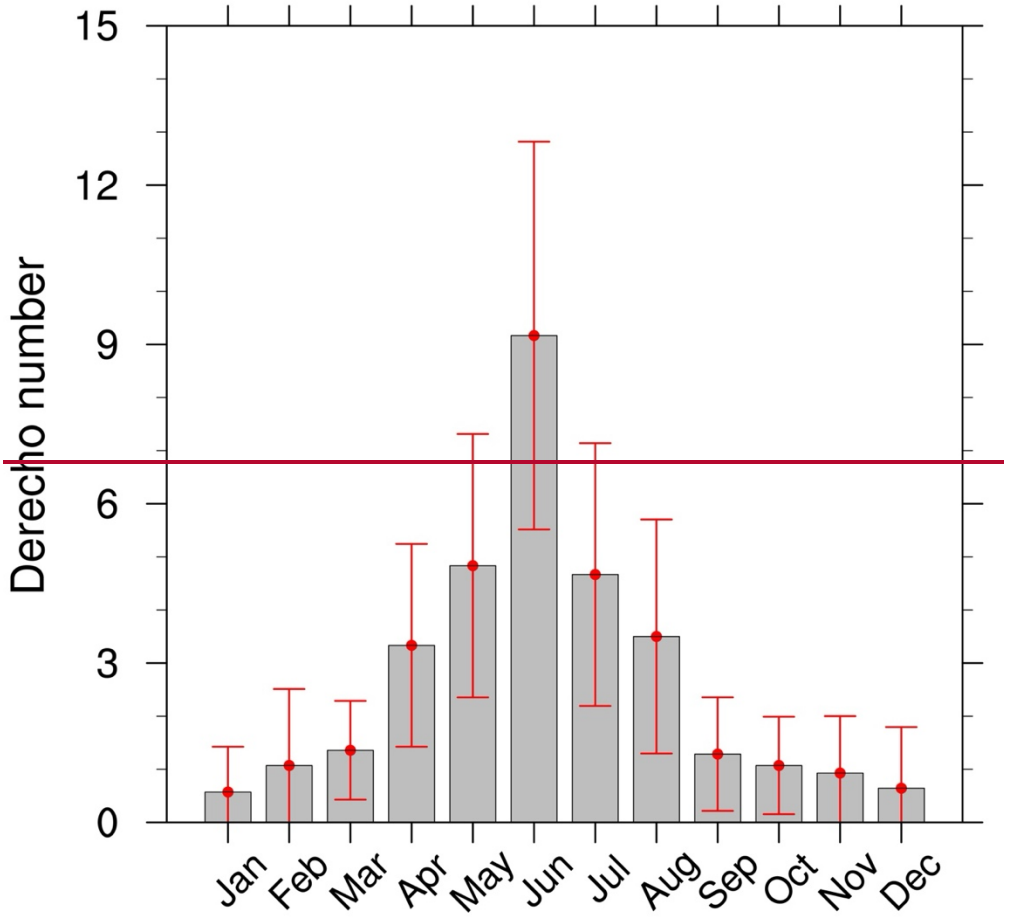
Derecho number
15
12
9
6
3
0
Jan
Feb
Mar
Apr
May
Jun
Jul
Aug
Sep
Oct
Nov
Dec

808

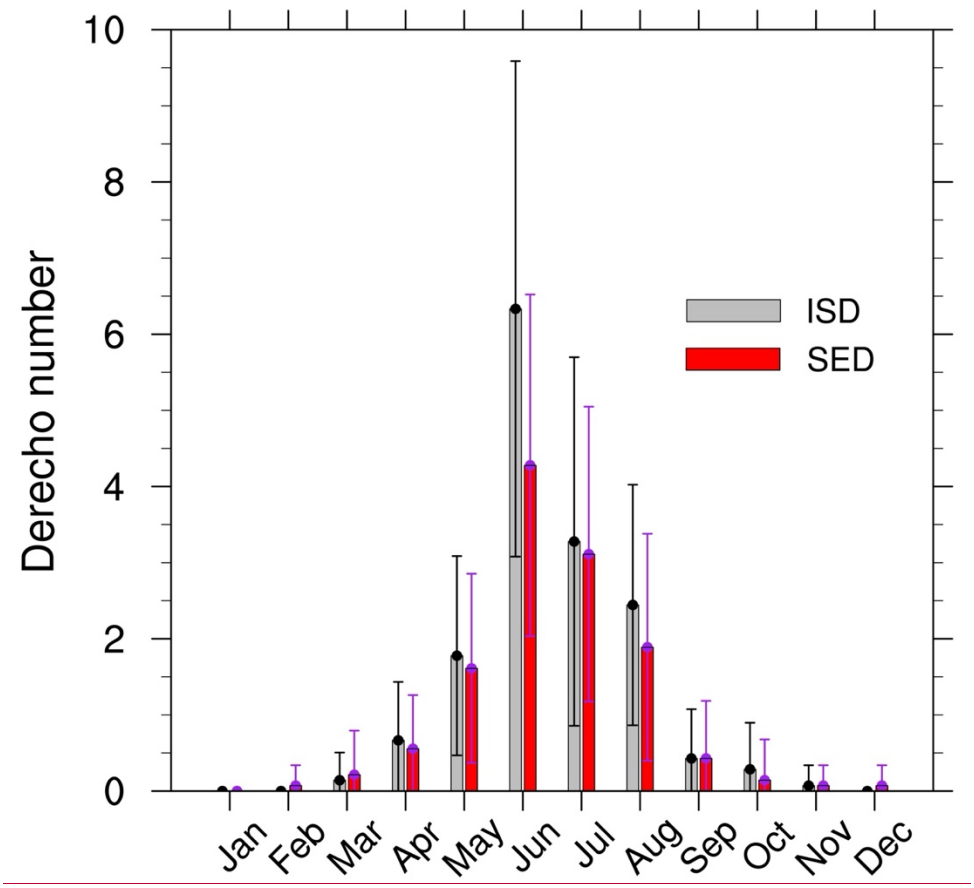

Figure ~~11~~10. Yearly averaged monthly variations of the derecho numbers between 2004 and 2021. The error bars denote standard deviations. Gray is for ISD-based derechos, and red colors indicate SED-based derechos.

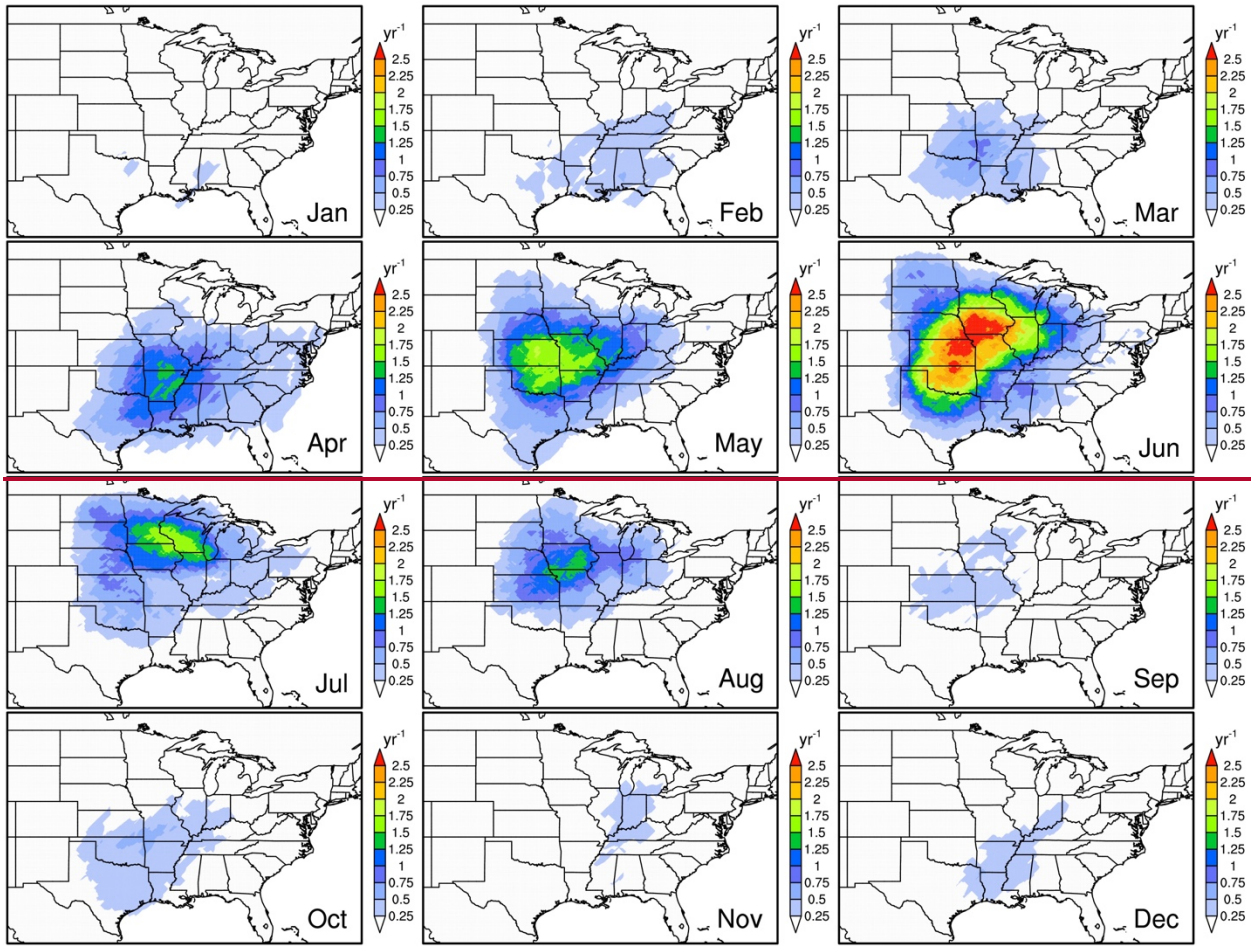
Jan
Feb
Mar
Apr
May
Jun
Jul
Aug
Sep
Oct
Nov
Dec
yr-1
2.5
2.25
2
1.75
1.5
1.25
1
0.75
0.5
0.25

812

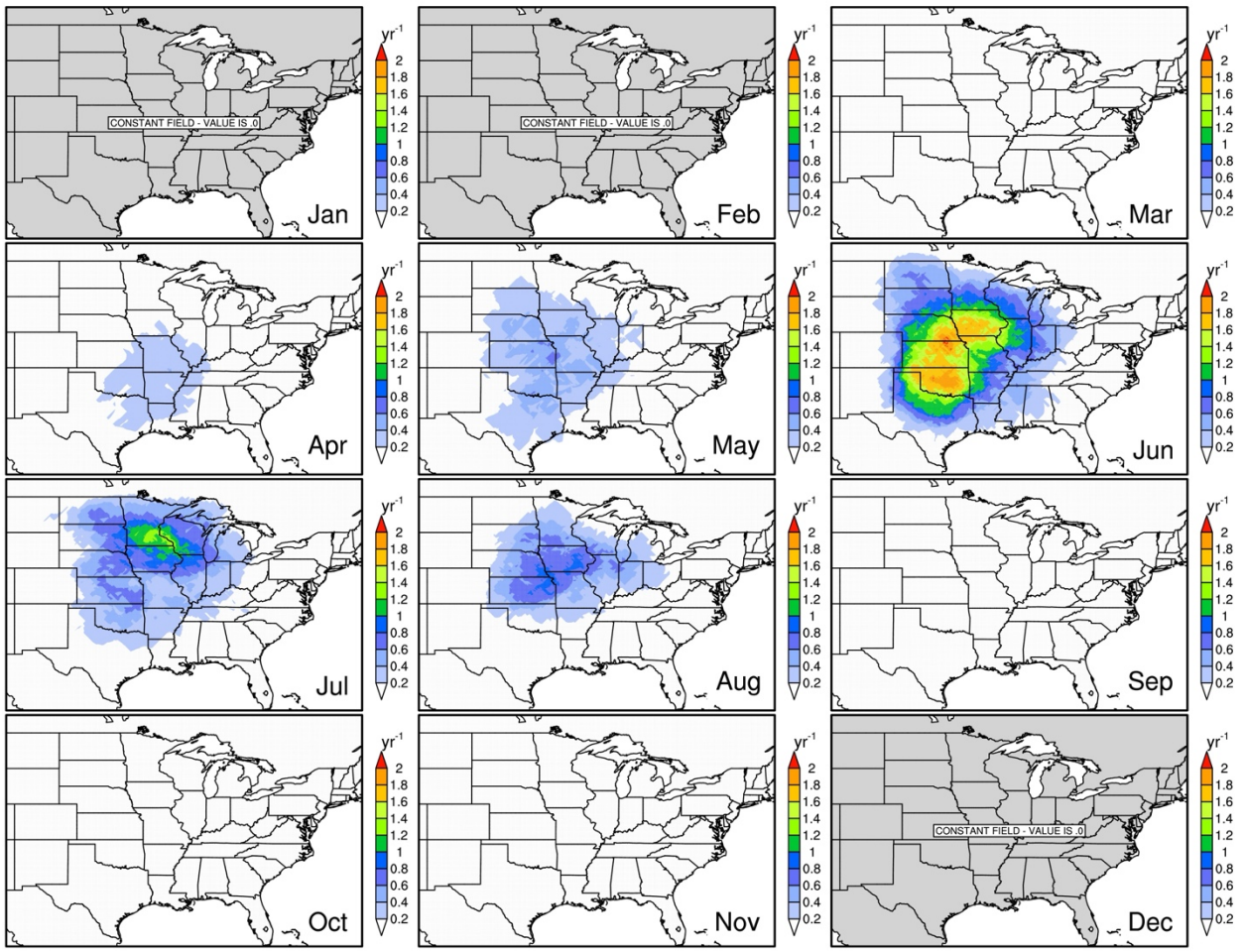

Figure ~~12~~11. Same as Figure ~~10~~9 but for yearly averaged monthly derecho numbers (ISD-based) over ~~2014~~2004-2021.

6.3 Wind damage characteristics

We examine the contributions of DMCSs and derechos ~~and DFs~~ to ~~all the~~ISD damaging gust reports in the United States ~~area of the~~within our dataset ~~domain between~~from 2004 ~~and~~to 2021 ~~in~~ (Figures ~~13~~12, S2, and S8~~.~~). Overall, MCSs contribute about ~~36.8~~15.6% of ~~the~~all damaging gust reports, ~~but most occur~~with the vast majority occurring east of the Rocky Mountains. On average, ~~derechos and DFs~~DMCSs contribute ~~19.2%~~4.0%, and ~~16.5~~derechos contribute 3.1% of ~~the~~all damaging gust occurrences~~, respectively. In other words,~~ . This indicates that about ~~half~~one quarter of the damaging gusts associated with MCS events are ~~related to derechos.~~linked to DMCSs, much higher than the fraction (~3.5%) of DMCSs in MCSs. This finding aligns with the higher probabilities of extreme gusts in the gust

speed PDF of DMCSs compared to general MCSs, indicating that DMCSs are more likely to produce extreme gusts than general MCSs (Figure S9). Understanding the ~~underlying~~ mechanisms behind their contrast will be ~~our~~a key focus ~~in~~of a follow-up study. ~~In addition, most (> 80%) derecho generated~~Additionally, approximately 75% of DMCS-associated damaging gusts occur during the ~~DF periods, justifying using DF in~~ derecho period, reinforcing the validity of our derecho definition~~, consistent with the larger probabilities of extreme gusts in the gust speed PDF of DFs than that of derechos in Figure S9. The gust speed PDFs for MCSs and derechos indicate that derechos are more favorable for producing extreme gusts than MCSs (Figure S9). Moreover, as~~. As expected, the highest contributions of derechos to damaging gust reports are ~~the highest~~found in the Great Plains~~,~~ and Midwest~~, and Lower Mississippi Valley (~~ (Figure 12).

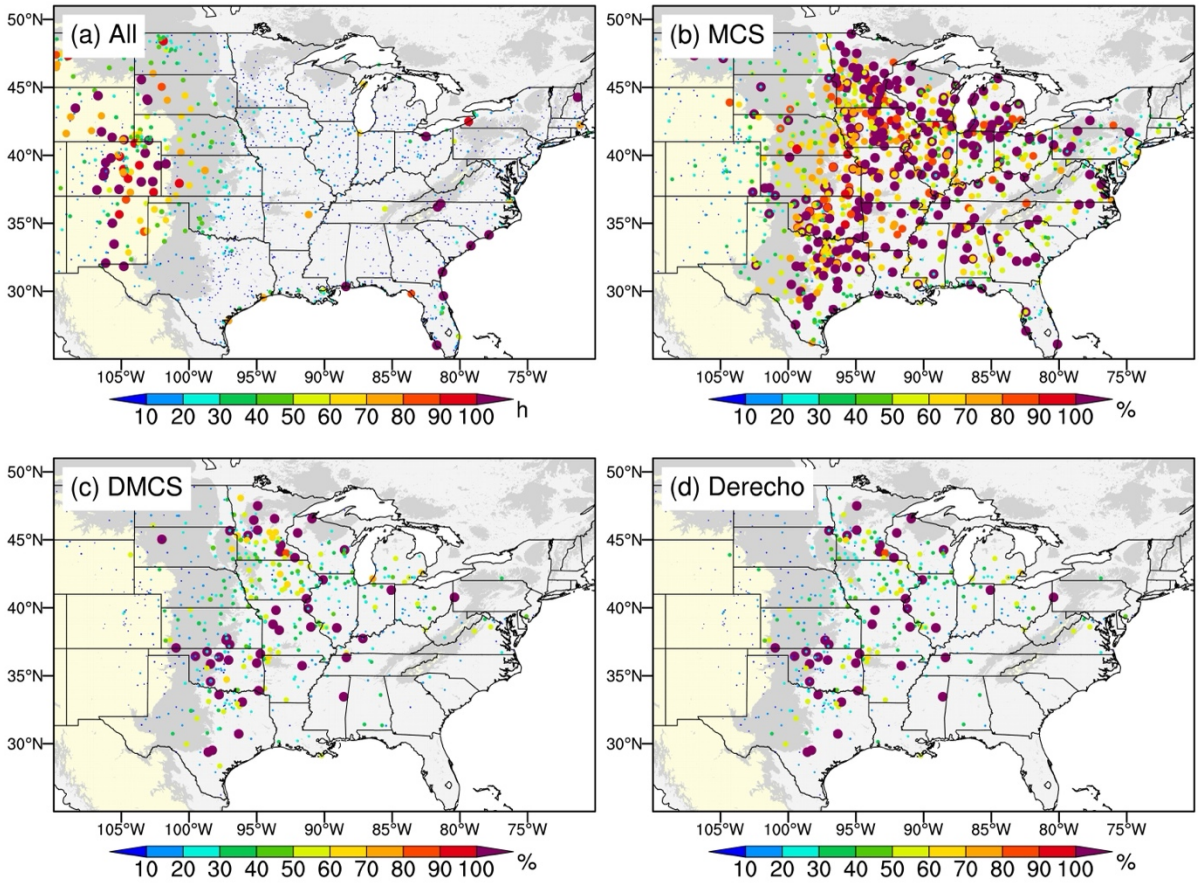

Figure ~~13).~~

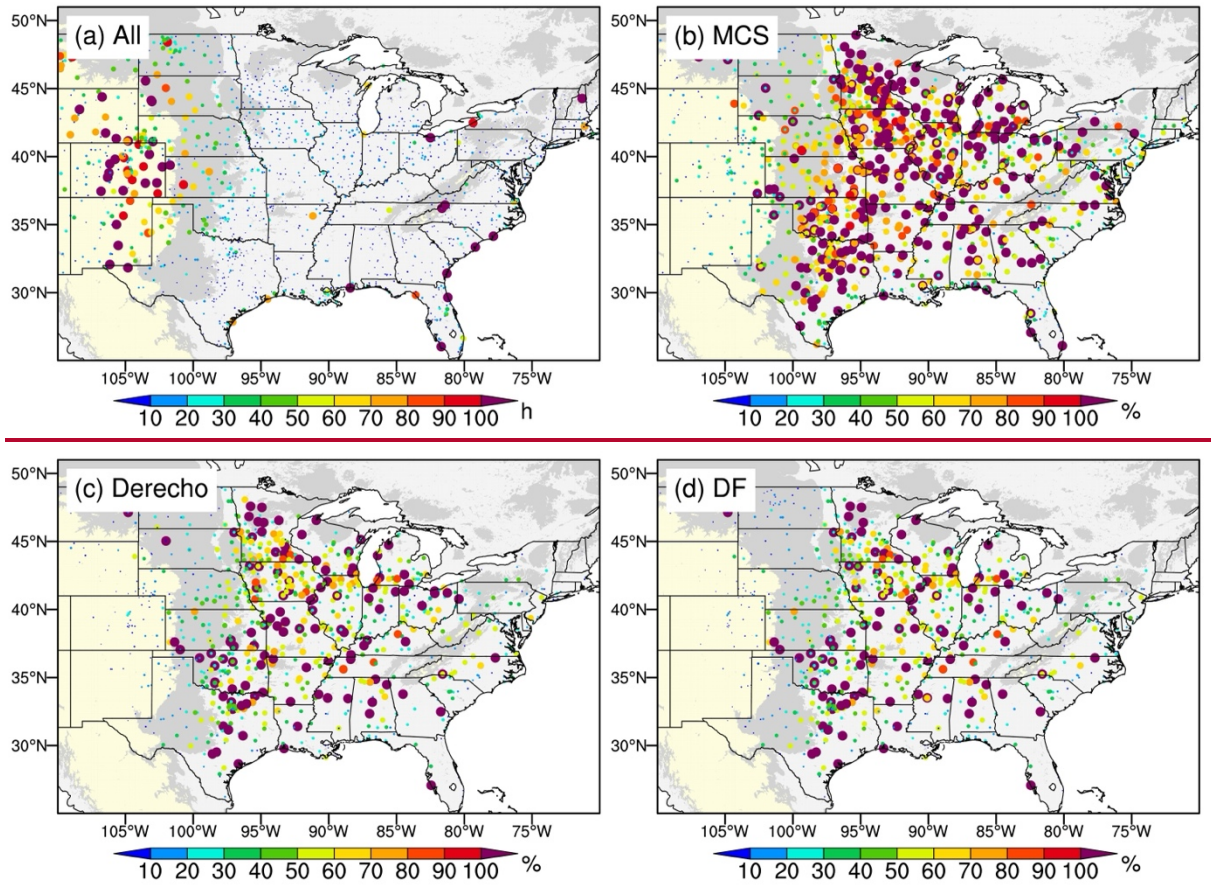

~~Figure 13~~12. (a) The total numbers of damaging gust occurrences between 2004 and 2021 at ISD weather stations over the United States east of the Rocky Mountains. (b) Relative contributions of MCS events to the damaging gust occurrences in (a). (c) is the same as (b) but for relative contributions of ~~derechos~~DMCSs. (d) is the same as (c), but ~~we only consider the DF periods when counting the derecho-associated damaging gust occurrences.~~ for derechos. Similar to Figure 5, we exclude non-derecho-producing MCS events overlapping with TCs in (b). The dot sizes are proportional to the corresponding values. Light-yellow shading denotes an elevation greater than 1000 m; light-gray shading denotes an elevation between 400 m and 1000 m; and smoke-white shading denotes an elevation less than 400 m. Background white is for oceans and lakes.

7 Data availability

The final ISD-based and SED-based derecho and DMCS dataset ~~and~~, along with the corresponding user guide ~~are~~, is publicly available at ~~https://doi.org/10.5281/zenodo.10884046~~ https://doi.org/10.5281/zenodo.14835362 (Li et al., ~~2024~~2025). The ~~original format of the data files is NetCDF-4, and we compress them for each year so that the~~ dataset is ~~easily accessible.~~stored in NetCDF-4 format and compressed by year for easier access. The user guide ~~contains~~provides a detailed description

of the data files ~~to help users understand~~, ensuring that users can effectively navigate and utilize the dataset.

For each pair of derecho and DMCS, the dataset ~~provides~~includes two visualization figures ~~displaying~~(one for derecho and the one for the accompanying DMCS) illustrating the temporal evolutions of Z_{Hmax}, precipitation, wind speed, and gust speed ~~during its entire lifetime and DF period~~throughout their respective lifetimes (e.g., Figures ~~14~~13 and S10). ~~The~~These figures ~~are helpful for~~ offer users ~~to understand~~an immediate understanding of the basic characteristics of ~~the derechos immediately. Notably, the~~ each derecho and DMCS. The dataset also contains all the derecho-associated gust ~~speed measurements, so~~speeds and various parameter values used in the derecho definition. This allows users ~~can~~to further ~~separate the~~categorize derechos ~~into different intensities, as in~~by intensity or type, following approaches similar to Coniglio and Stensrud (2004).

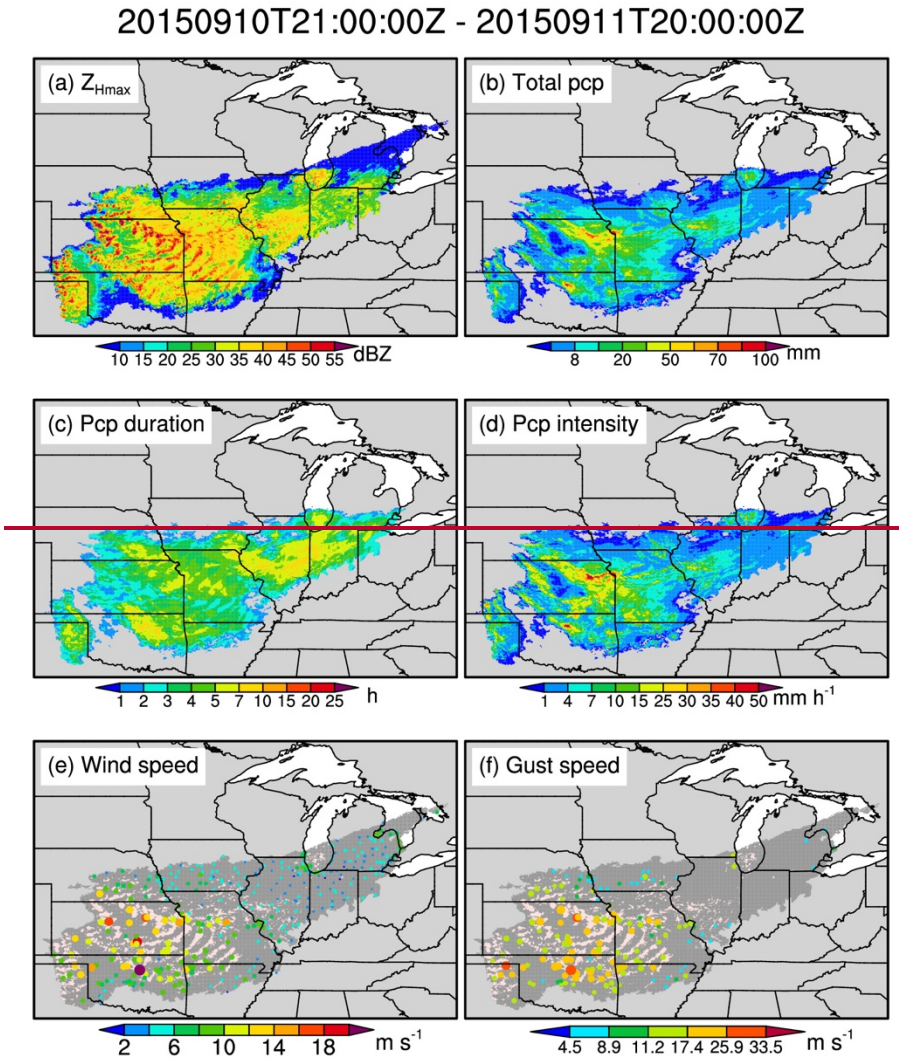

For researchers interested in applying the segmentation CNN for bow echo detection in different regions or time periods, or in leveraging the CNN-identified bow echoes for other studies, we provide access to the bow echo segmentation code and datasets at https://doi.org/10.5281/zenodo.10822721 (Geiss et al., 2024). This repository includes the trained CNN weights and detailed usage instructions. Additionally, a video supplement demonstrating the bow echo segmentation scheme is available at https://youtu.be/iHWY_OhaVUo and is permanently archived in the above Zenodo repository.

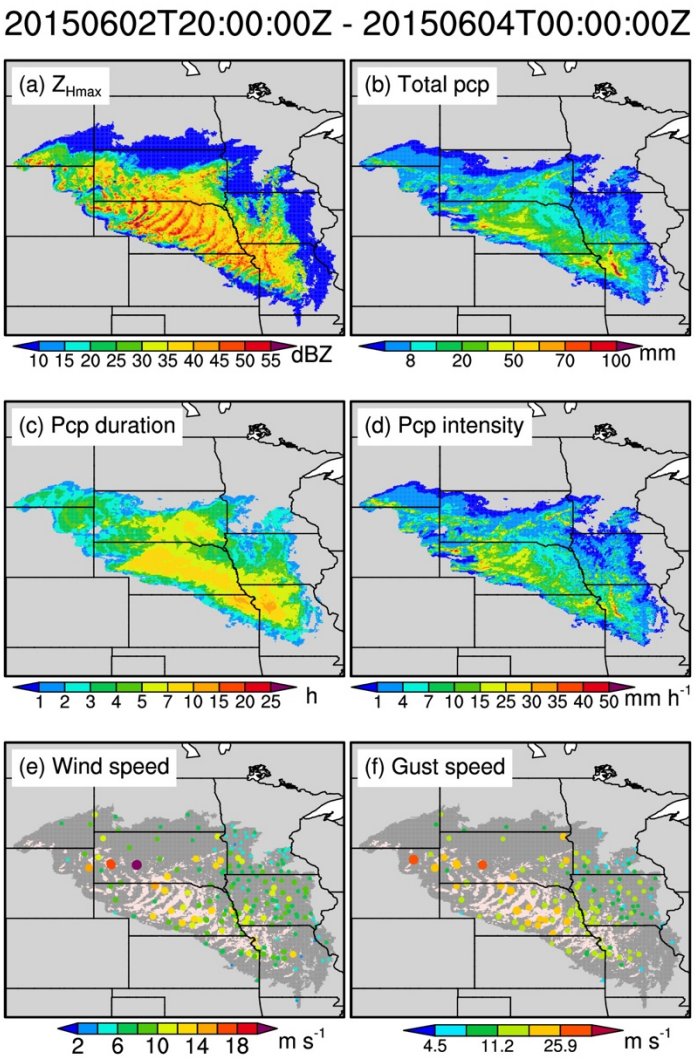

Figure ~~14~~13. Similar to Figure 1 but for the spatial evolutions of (a) Z_{Hmax}, (b) total accumulated precipitation, (c) precipitation duration, (d) mean precipitation intensity, (e) hourly maximum wind speed, and (f) hourly maximum gust speed ~~during the entire lifetime of~~for a ~~derecho~~ISD-based DMCS that occurred on ~~10–11 September~~2-4 June 2015. In (e) and (f), the misty rose shading corresponds to areas with $Z_{Hmax} \geq 40$ dBZ, and the dark gray shading refers to ~~derecho~~DMCS coverage with $Z_{Hmax} < 40$ dBZ. The figure title refers to the ~~derecho~~DMCS timing range.

8 Conclusions

This study presents a high-resolution (4 km and hourly) observational derecho dataset covering the United States east of the Rocky Mountains from 2004 to 2021. We develop the dataset using ~~an~~a combination of:

- An MCS dataset generated by the PyFLEXTRKR ~~software, a machine-learning-based identification of bow~~ ,
- Bow echoes~~, ISD hourly~~ identified by a semantic segmentation CNN,
- Hourly gust speed ~~measurements~~datasets from ISD or SED, and ~~physically~~
- Physically based derecho identification criteria. ~~The evaluation~~

We evaluate the dataset and its potential uncertainties ~~of the dataset are discussed.~~. The final dataset ~~contains 556~~identifies 274 derechos~~, most of which are~~ using ISD gust measurements and 220 derechos using SED gust reports, with most events occurring in the warm season (April-August). Analyses indicate that derechos ~~preferably~~preferentially occur in the Great Plains and Midwest~~. Areas with the most frequent derechos show a northeastward shift~~, with regions of highest frequency shifting northward from April to August. Derechos contribute ~~19.2~~3.1% of ISD land-based damaging gusts over the United States between 2004 and 2021. ~~About half~~Additionally, approximately 20% of MCS-associated damaging gusts are produced by derechos.

As the first derecho dataset that ~~uses~~integrates machine-learning-based bow echo identification ~~of bow echoes~~, physically based definition criteria, and two types of surface ~~station measured gust speeds, it provides~~gust speed data, the dataset serves as an independent reference for derecho climatology ~~compared to~~, complementing previous studies. ~~In addition~~Beyond climatological analyses, the ~~derecho~~ dataset can be used to ~~investigate~~:

- Investigate the derecho initiation and development mechanisms, ~~the environments~~
- Examine the environmental conditions that ~~facilitate the~~ promote derecho formation and intensification,
- Assess the impacts of derechos~~, and the damage of derechos to~~ on human ~~security~~safety and property~~. Moreover, due to its high spatiotemporal resolutions, the dataset can be used to select~~, and

- Select specific ~~derecho~~ events for case studies ~~and~~or to evaluate the numerical model simulations, thanks to its high spatiotemporal resolution.

Lastly, we emphasize that the automated derecho detection algorithm developed in this study is versatile and applicable to both observations and model results. The algorithm can be used to assess model performance and explore the impact of various factors on derechos (Kaminski et al., 2025).

Appendix A

For each bow echo in the derecho bow echo series, we use the formulas from the MATrix LABoratory (MATLAB) "regionprops" function (https://github.com/SBU-BMI/nscale/blob/master/original-matlab/features/regionprops.m; last access: January 28, 2025) to calculate its orientation. Then we apply the three-sigma rule to the orientations to remove outliers until all the rest orientations lie within three standard deviations of their mean. The mean is the average bow echo orientation. Implementing the three-sigma rule aims to minimize the adverse impact of the segmentation CNN identification uncertainties on calculating the averaged bow echo orientation.

The bow echo series' propagation direction and speed are calculated as follows. Firstly, we compute the moving direction and speed between any two consecutive bow echoes from the series. As exemplified in Figure A1, we assume that the bow echo at time t_1 would move to the location of bow echo t_1' at time t_2 if the bow echo shape remained unchanged. The location of bow echo t_1' is determined by its spatial correlation coefficient with bow echo t_2, and the location with the largest spatial correlation coefficient is what we want. Since bow echoes t_1 and t_1' have the same shape, it is straightforward to calculate the moving direction and speed between them, which are considered the moving direction and speed between bow echoes t_1 and t_2. Compared to using the centroid points of bow echoes t_1 and t_2, our approach can reduce the calculation bias when bow echoes t_1 and t_2 have distinct shapes and sizes. After we obtain all the moving directions and speeds between any two consecutive bow echoes, we apply the 1.5 ×

Interquartile Range (IQR) rule to remove outliers, considering potential CNN bow echo identification errors. Lastly, the median of the remaining moving speed values is considered the bow echo series' propagation speed, while the average of the remaining move direction values is considered the bow echo series' propagation direction.

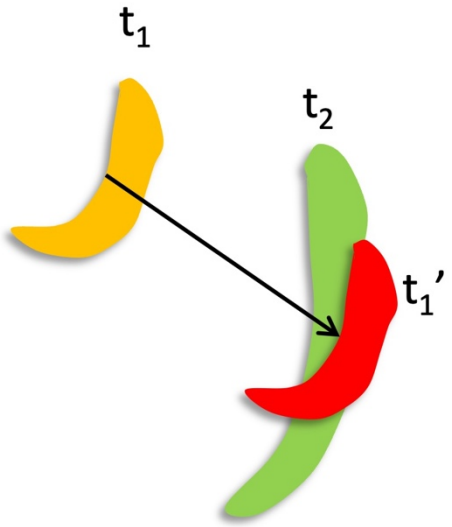

Figure A1. Schematic of the bow echo moving direction and speed calculation between two consecutive (t_1 and t_2) bow echoes. Bow echo t_1' is the same as bow echo t_1 but at a different location so that the spatial correlation coefficient between bow echoes t_1' and t_2 reaches the maximum. The moving direction and speed between bow echoes t_1 and t_1' are considered the moving direction and speed between bow echoes t_1 and t_2.

We use wind speeds at 500 hPa from ERA5 to compute the background mean wind speed. Considering the potential spatiotemporal variability of 500-hPa winds, we only count wind speeds covered by bow echoes from the bow echo series during the corresponding period. In detail, at time t_i during the bow echo series period (t_1–t_n), we only consider winds at time t_i but covered by bow echoes from time t_{i+1} to $min(t_{i+3}, t_n)$. Here, we exclude the bow echo at time t_i to minimize the potential impact of the bow echo on the background environment, while using up to three hours (t_{i+1}–t_{i+3}) of bow echoes aims to reduce the potential spatial noise since a bow echo is often too small. We average all wind speeds obtained from the above procedure to derive the background mean wind speed.

Author Contributions

JL, ZF, and LRL designed the study. JL prepared the input files for PyFLEXTRKR, and ZF ran PyFLEXTRKR to generate the MCS dataset. JL and ZF generated the initial positive and negative bow echo samples. AG trained and validated the CNN model. AG applied the trained semantic segmentation CNN to identify bow echoes from the MCS dataset with discussions with JL and ZF. JL defined and identified derechos with discussions with ZF. JL evaluated the derecho dataset and manually examined the data. JL analyzed the derecho climatology with discussions with ZF. JL wrote the manuscript except for the machine-learning part which was written by AG. All co-authors reviewed the manuscript.

Competing Interests

The authors declare that they have no conflict of interest.

Acknowledgments

The NOAA SPC derechos and near-derechos are available at https://www.spc.noaa.gov/misc/AbtDerechos/annualevents.htm (last access: November 17, 2023). The named derechos we use to generate bow echo samples are from https://en.wikipedia.org/wiki/List_of_derecho_events (last access: 19 March 2023). The elevation data is from http://iridl.ldeo.columbia.edu/SOURCES/.NOAA/.NGDC/.GLOBE/ (last access: March 7, 2024). The IBTrACS Version 4 TC data over the North Atlantic basin is from https://doi.org/10.25921/82ty-9e16 (Knapp et al., 2018). Thank Drs. Israel L. Jirak, Brian J. Squitieri, and Andrew R. Wade from NOAA SPC for discussing the derecho definition criteria with us.

~~The bow echo segmentation code and datasets are available at https://doi.org/10.5281/zenodo.10822721 (Geiss et al., 2024). This repository includes the trained CNN weights and instructions for use. A video~~

~~supplement showing the bow echo segmentation scheme in use can be viewed at~~

~~https://youtu.be/iHWY_OhaVUo and is permanently archived in the above Zenodo repository.~~

Financial support

This research is supported by the Regional and Global Model Analysis and Multisector Dynamics program areas of the U.S. Department of Energy Office of Science Biological and Environmental Research as part of the HyperFACETS project. PNNL is operated for the Department of Energy by Battelle Memorial Institute under Contract DE-AC05-76RL01830.

References

Adams-Selin, R. D. and Johnson, R. H.: Mesoscale surface pressure and temperature features associated with bow echoes, Monthly ~~weather review~~Weather Review, 138, 212-227, https://doi.org/10.1175/2009MWR2892.1, 2010.

Ardon-Dryer, K., Gill, T. E., and Tong, D. Q.: When a Dust Storm Is Not a Dust Storm: Reliability of Dust Records From the Storm Events Database and Implications for Geohealth Applications, GeoHealth, 7, e2022GH000699, https://doi.org/10.1029/2022GH000699, 2023.

Ashley, W. S. and Mote, T. L.: Derecho hazards in the United States, Bulletin of the American Meteorological Society, 86, 1577-1592, https://doi.org/10.1175/BAMS-86-11-1577, 2005.

Bardis, M., Houshyar, R., Chantaduly, C., Ushinsky, A., Glavis-Bloom, J., Shaver, M., Chow, D., Uchio, E., and Chang, P.: Deep learning with limited data: Organ segmentation performance by U-Net, Electronics, 9, 1199, https://doi.org/10.3390/electronics9081199, 2020.

Bentley, M. L. and Mote, T. L.: A climatology of derecho-producing mesoscale convective systems in the central and eastern United States, 1986–95. Part I: Temporal and spatial distribution, Bulletin of the American Meteorological Society, 79, 2527-2540, https://doi.org/10.1175/1520-0477(1998)079<2527:ACODPM>2.0.CO;2, 1998.

Bentley, M. L. and Sparks, J. A.: A 15 yr climatology of derecho-producing mesoscale convective systems over the central and eastern United States, Climate research, 24, 129-139, https://www.jstor.org/stable/24868368, 2003.

Bishop, C. M.: Pattern recognition and machine learning, Information Science and Statistics, 4, Springer, New York, NY, 2006.

Bowman, K. P. and Homeyer, C. R.: GridRad - Three-Dimensional Gridded NEXRAD WSR-88D Radar Data, the National Center for Atmospheric Research, Computational and Information Systems Laboratory [dataset], https://doi.org/10.5065/D6NK3CR7, 2017 (last access: 3 November 2022).

CDIACS/EOL/NCAR/UCAR and CPC/NCEP/NWS/NOAA: NCEP/CPC Four Kilometer Precipitation Set, Gauge and Radar, the National Center for Atmospheric Research, Computational and Information Systems Laboratory [dataset], https://doi.org/10.5065/D69Z93M3, 2000 (last access: 31 October 2022).

Coniglio, M. C. and Stensrud, D. J.: Interpreting the climatology of derechos, Weather and forecasting, 19, 595-605, https://doi.org/10.1175/1520-0434(2004)019<0595:ITCOD>2.0.CO;2, 2004.

Corfidi, S. F., Coniglio, M. C., Cohen, A. E., and Mead, C. M.: A proposed revision to the definition of "derecho", Bulletin of the American Meteorological Society, 97, 935-949, https://doi.org/10.1175/BAMS-D-14-00254.1, 2016.

Evans, J. S. and Doswell, C. A.: Examination of derecho environments using proximity soundings, Weather and Forecasting, 16, 329-342, https://doi.org/10.1175/1520-0434(2001)016<0329:EODEUP>2.0.CO;2, 2001.

Feng, Z.: Mesoscale convective system (MCS) database over United States (V3) [dataset], https://doi.org/10.5439/1571643, 2024 (last access: 25 Feburary 2025).

Feng, Z., Hardin, J., Barnes, H. C., Li, J., Leung, L. R., Varble, A., and Zhang, Z.: PyFLEXTRKR: a flexible feature tracking Python software for convective cloud analysis, Geoscientific Model Development, 16, 2753-2776, https://doi.org/10.5194/gmd-16-2753-2023, 2023.

Feng, Z., Houze, R. A., Leung, L. R., Song, F., Hardin, J. C., Wang, J., Gustafson, W. I., and Homeyer, C. R.: Spatiotemporal characteristics and large-scale environments of mesoscale convective systems east of the Rocky Mountains, Journal of Climate, 32, 7303-7328, https://doi.org/10.1175/JCLI-D-19-0137.1, 2019.

Feng, Z., Leung, L. R., Liu, N., Wang, J., Houze Jr, R. A., Li, J., Hardin, J. C., Chen, D., and Guo, J.: A global high-resolution mesoscale convective system database using satellite-derived cloud tops, surface precipitation, and tracking, Journal of Geophysical Research: Atmospheres, 126, e2020JD034202, https://doi.org/10.1029/2020JD034202, 2021.

Fujita, T. T.: Proposed characterization of tornadoes and hurricanes by area and intensity, ~~1971.~~https://ntrs.nasa.gov/api/citations/19720008829/downloads/19720008829.pdf, 1971.

Galea, D., Ma, H.-Y., Wu, W.-Y., and Kobayashi, D.: Deep Learning Image Segmentation for Atmospheric Rivers, Artificial Intelligence for the Earth Systems, 3, 230048, https://doi.org/10.1175/AIES-D-23-0048.1, 2024.

Geiss, A. and Hardin, J. C.: Radar super resolution using a deep convolutional neural network, Journal of Atmospheric and Oceanic Technology, 37, 2197-2207, https://doi.org/10.1175/JTECH-D-20-0074.1, 2020.

Geiss, A., Li, J., Feng, Z., and Leung, L. R.: Bow echo detection and segmentation, Zenodo [dataset], https://doi.org/10.5281/zenodo.10822721, 2024 (last access: 15 March 2024).

Guastini, C. T. and Bosart, L. F.: Analysis of a progressive derecho climatology and associated formation environments, Monthly Weather Review, 144, 1363-1382, https://doi.org/10.1175/MWR-D-15-0256.1, 2016.

Hersbach, H., Bell, B., Berrisford, P., Biavati, G., Horányi, A., Muñoz Sabater, J., Nicolas, J., Peubey, C., Radu, R., Rozum, I., Schepers, D., Simmons, A., Soci, C., Dee, D., and Thépaut, J.-N.: ERA5 hourly data on single levels from 1940 to present, Copernicus Climate Change Service (C3S) Climate Data Store (CDS) [dataset], https://doi.org/10.24381/cds.adbb2d47, 2023 (last access: 1 November 2022).

Huang, G., Liu, Z., Pleiss, G., Van Der Maaten, L., and Weinberger, K. Q.: Convolutional networks with dense connectivity, IEEE transactions on pattern analysis and machine intelligence, 44, 8704-8716, https://doi.org/10.1109/TPAMI.2019.2918284, 2019.

Huang, H., Lin, L., Tong, R., Hu, H., Zhang, Q., Iwamoto, Y., Han, X., Chen, Y.-W., and Wu, J.: Unet 3+: A full-scale connected unet for medical image segmentation, ICASSP 2020-2020 IEEE international conference on acoustics, speech and signal processing (ICASSP), 1055-1059, https://doi.org/10.1109/ICASSP40776.2020.9053405, 2020.

Janowiak, J., Joyce, B., and Xie, P.: NCEP/CPC L3 Half Hourly 4km Global (60S - 60N) Merged IR V1, Goddard Earth Sciences Data and Information Services Center (GES DISC) [dataset], https://doi.org/10.5067/P4HZB9N27EKU, 2017 (last access: 27 September 2022).

Johns, R. H. and Hirt, W. D.: Derechos: Widespread convectively induced windstorms, Weather and Forecasting, 2, 32-49, https://doi.org/10.1175/1520-0434(1987)002<0032:DWCIW>2.0.CO;2, 1987.

Kaminski, K., Ashley, W. S., Haberlie, A. M., and Gensini, V. A.: Future Derecho Potential in the United States, Journal of Climate, 38, 3-26, https://doi.org/10.1175/JCLI-D-23-0633.1, 2025.

Ketkar, N.: Introduction to keras, Deep learning with ~~python~~Python: a hands-on introduction, 97-111, https://doi.org/10.1007/978-1-4842-2766-4_7, 2017.

Kingma, D. P. and Ba, J.: Adam: A method for stochastic optimization, arXiv preprint arXiv:1412.6980, https://doi.org/10.48550/arXiv.1412.6980, 2014.

Knapp, K. R., Diamond, H. J., Kossin, J. P., Kruk, M. C., and Schreck, C. J. I.: International Best Track Archive for Climate Stewardship (IBTrACS) Project, Version 4, [North Atlantic], NOAA National Centers for Environmental Information [dataset], https://doi.org/10.25921/82ty-9e16, 2018 (last access: 5 March 2024).

Knapp, K. R., Kruk, M. C., Levinson, D. H., Diamond, H. J., and Neumann, C. J.: The international best track archive for climate stewardship (IBTrACS) unifying tropical cyclone data, Bulletin of the American Meteorological Society, 91, 363-376, https://doi.org/10.1175/2009BAMS2755.1, 2010.

Kumler-Bonfanti, C., Stewart, J., Hall, D., and Govett, M.: Tropical and extratropical cyclone detection using deep learning, Journal of Applied Meteorology and Climatology, 59, 1971-1985, https://doi.org/10.1175/JAMC-D-20-0117.1, 2020.

Lagerquist, R., Turner, D., Ebert-Uphoff, I., Stewart, J., and Hagerty, V.: Using deep learning to emulate and accelerate a radiative transfer model, Journal of Atmospheric and Oceanic Technology, 38, 1673-1696, https://doi.org/10.1175/JTECH-D-21-0007.1, 2021.

Li, J., Feng, Z., Qian, Y., and Leung, L. R.: A high-resolution unified observational data product of mesoscale convective systems and isolated deep convection in the United States for 2004–2017, Earth Syst. Sci. Data, 13, 827-856, https://doi.org/10.5194/essd-13-827-2021, 2021.

Li, J., Geiss, A., Feng, Z., and Leung, L. R.: A derecho climatology over the United States from 2004 to 2021, Zenodo [dataset], https://doi.org/10.5281/zenodo.~~10884046, 2024~~14835362, 2025 (last access: ~~27 March 2024~~7 February 2025).

Mounier, A., Raynaud, L., Rottner, L., Plu, M., Arbogast, P., Kreitz, M., Mignan, L., and Touzé, B.: Detection of bow echoes in kilometer-scale forecasts using a convolutional neural network, Artificial Intelligence for the Earth Systems, 1, e210010, https://doi.org/10.1175/AIES-D-21-0010.1, 2022.

NOAA/NCEI: Global Hourly - Integrated Surface Database (ISD), the National Oceanic and Atmospheric Administration (NOAA) National Centers for Environmental Information (NCEI) [dataset], https://www.ncei.noaa.gov/data/global-hourly/archive/isd/, 2001 (last access: 21 January 2023).

NOAA/NCEI: Federal Climate Complex Data Documentation For Integrated Surface Data (ISD), 126, https://www.ncei.noaa.gov/data/global-hourly/doc/isd-format-document.pdf, 2018.

NOAA/NCEI: Storm Events Database [dataset], https://www.ncdc.noaa.gov/stormevents/, 2025 (last access: 27 August 2024).

Ouali, Y., Hudelot, C., and Tami, M.: An overview of deep semi-supervised learning, arXiv preprint arXiv:2006.05278, https://doi.org/10.48550/arXiv.2006.05278, 2020.

Peláez-Vegas, A., Mesejo, P., and Luengo, J.: A Survey on Semi-Supervised Semantic Segmentation, arXiv preprint arXiv:2302.09899, https://doi.org/10.48550/arXiv.2302.09899, 2023.

Ronneberger, O., Fischer, P., and Brox, T.: U-net: Convolutional networks for biomedical image segmentation, Medical Image Computing and Computer-Assisted Intervention–MICCAI 2015: 18th International Conference, Munich, Germany, October 5-9, 2015, Proceedings, Part III 18, 234-241, https://doi.org/10.1007/978-3-319-24574-4_28,

Santos, R. P. d.: Some comments on the reliability of NOAA's Storm Events Database, arXiv preprint, https://doi.org/10.48550/arXiv.1606.06973, 2016.

Sha, Y., Gagne II, D. J., West, G., and Stull, R.: Deep-learning-based gridded downscaling of surface meteorological variables in complex terrain. Part I: Daily maximum and minimum 2-m temperature, Journal of Applied Meteorology and Climatology, 59, 2057-2073, https://doi.org/10.1175/JAMC-D-20-0057.1, 2020.

Smith, A., Lott, N., and Vose, R.: The integrated surface database: Recent developments and partnerships, Bulletin of the American Meteorological Society, 92, 704-708, https://doi.org/10.1175/2011BAMS3015.1, 2011.

Squitieri, B. J., Wade, A. R., and Jirak, I. L.: A historical overview on the science of derechos: part I: identification, climatology, and societal impacts, Bulletin of the American Meteorological Society, 104, E1709-E1733, https://doi.org/10.1175/BAMS-D-22-0217.1, 2023.

Starzec, M., Homeyer, C. R., and Mullendore, G. L.: Storm labeling in three dimensions (SL3D): A volumetric radar echo and dual-polarization updraft classification algorithm, Monthly Weather Review, 145, 1127-1145, https://doi.org/10.1175/MWR-D-16-0089.1, 2017.

Taha, A. A. and Hanbury, A.: Metrics for evaluating 3D medical image segmentation: analysis, selection, and tool, BMC medical imaging, 15, 1-28, https://doi.org/10.1186/s12880-015-0068-x, 2015.

Van Engelen, J. E. and Hoos, H. H.: A survey on semi-supervised learning, Machine learning, 109, 373-440, https://doi.org/10.1007/s10994-019-05855-6, 2020.

Weisman, M. L.: The genesis of severe, long-lived bow echoes, Journal of the ~~atmospheric sciences~~Atmospheric Sciences, 50, 645-670, https://doi.org/10.1175/1520-0469(1993)050<0645:TGOSLL>2.0.CO;2, 1993.

Weyn, J. A., Durran, D. R., Caruana, R., and Cresswell-Clay, N.: Sub-seasonal forecasting with a large ensemble of deep-learning weather prediction models, Journal of Advances in Modeling Earth Systems, 13, e2021MS002502, https://doi.org/10.1029/2021MS002502, 2021.

White, C. H., Ebert-Uphoff, I., Haynes, J. M., and Noh, Y.-J.: Super-Resolution of GOES-16 ABI Bands to a Common High Resolution with a Convolutional Neural Network, Artificial Intelligence for the Earth Systems, https://doi.org/10.1175/AIES-D-23-0065.1, 2024.

Whitehall, K., Mattmann, C. A., Jenkins, G., Rwebangira, M., Demoz, B., Waliser, D., Kim, J., Goodale, C., Hart, A., and Ramirez, P.: Exploring a graph theory based algorithm for automated identification and characterization of large mesoscale convective systems in satellite datasets, Earth Science Informatics, 8, 663-675, https://doi.org/10.1007/s12145-014-0181-3, 2015.

Supplementary information for

A derecho climatology (2004-2021) in the United States based on machine learning identification of bow echoes

Jianfeng Li[1, *], Andrew Geiss[1], Zhe Feng[1, *], L. Ruby Leung[1] Yun Qian[1], Wenjun Cui[2]

[1]Atmospheric, Climate, and Earth Sciences Division, Pacific Northwest National Laboratory, Richland, Washington, USA

[2]Cooperative Institute for Severe and High-Impact Weather Research and Operations, University of Oklahoma, Norman, Oklahoma, USA

[3]National Severe Storms Laboratory, National Oceanic and Atmospheric Administration, Norman, Oklahoma, USA

*Correspondence to Jianfeng Li (jianfeng.li@pnnl.gov) and Zhe Feng (zhe.feng@pnnl.gov)

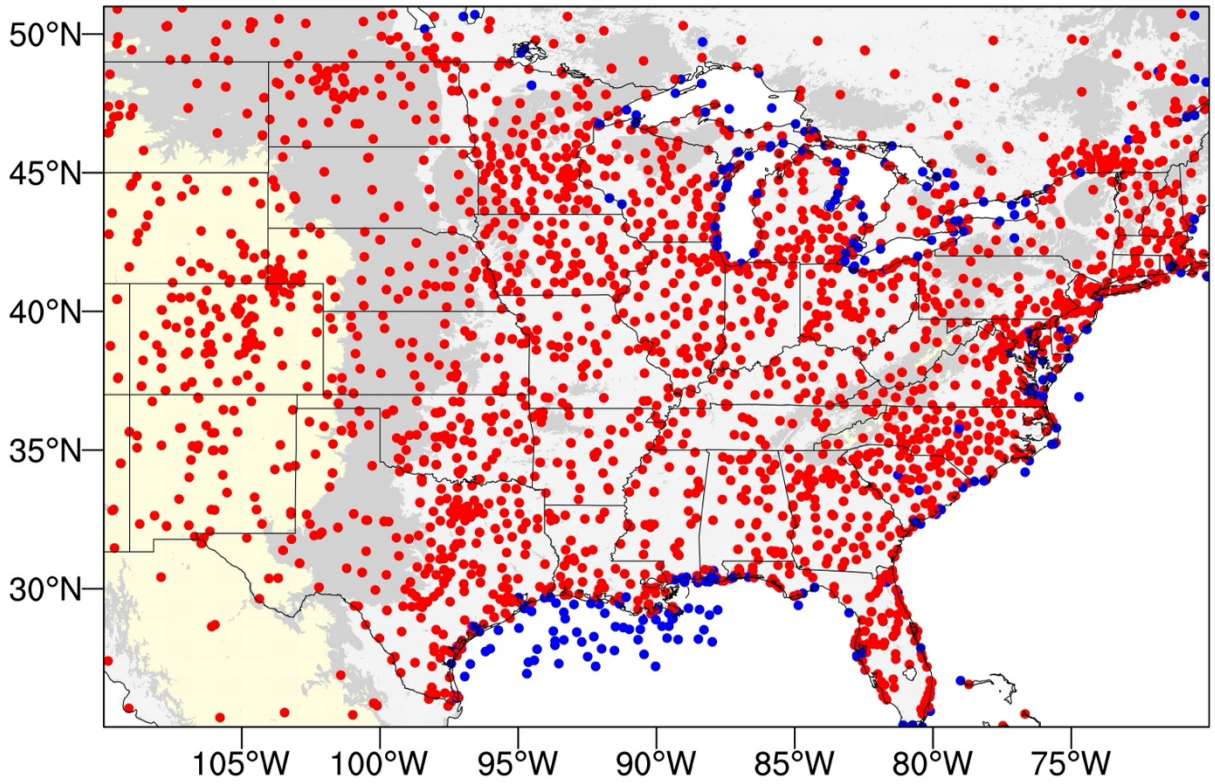

Figure S1. Locations of ISD gust speed observational sites used in the study. There are 4,260 sites, 3,954 of which are over land (red points), while the rest are over the ocean or lakes (blue points). We use the Advanced Research Weather Research and Forecasting (WRF) Preprocess System (WPS) to generate a 4-km land cover map to determine the land type associated with each observational site. Light-yellow shading denotes an elevation greater than 1000 m; light-gray shading denotes an elevation between 400 m and 1000 m; and smoke-white shading denotes an elevation less than 400 m. Background white is for the ocean and lakes.

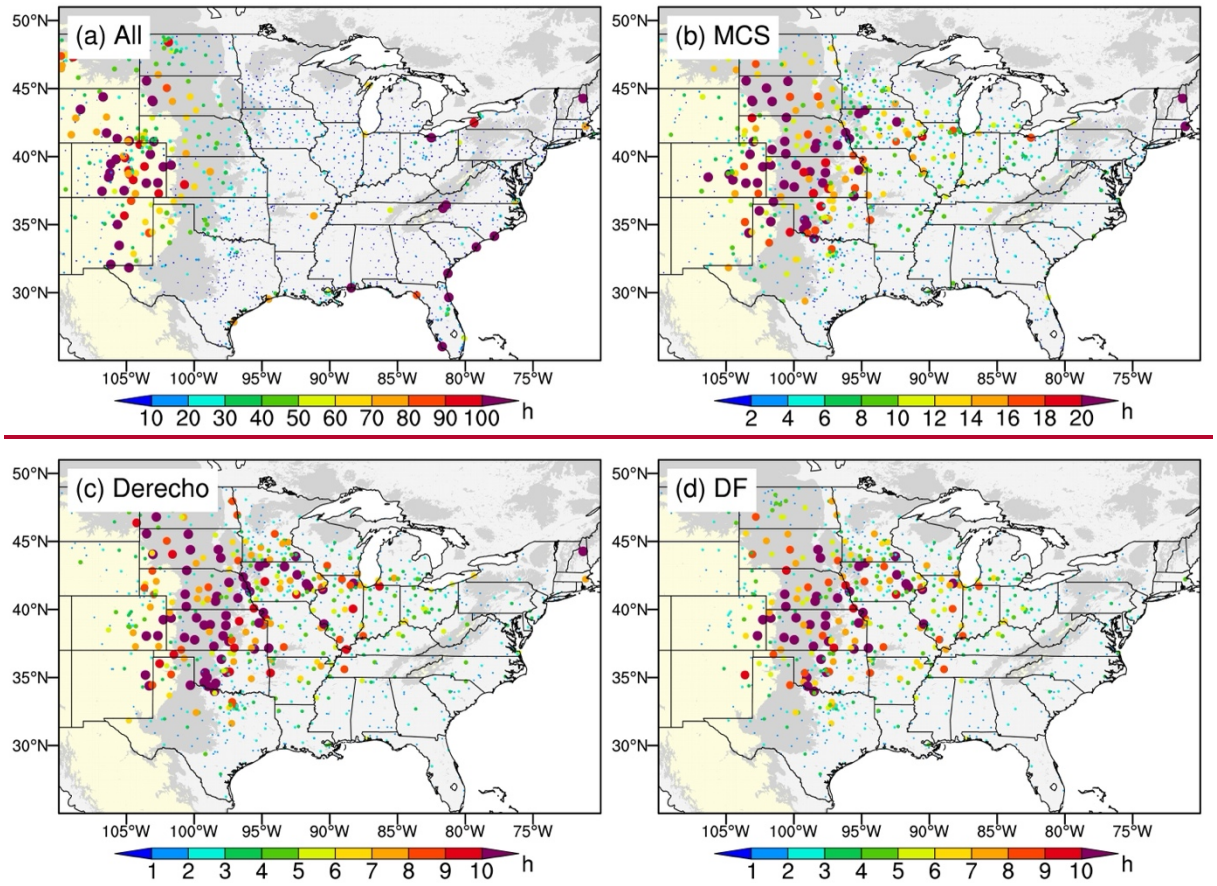
(a) All
(b) MCS
(c) Derecho
(d) DF
50°N
45°N
40°N
35°N
30°N
105°W 100°W 95°W 90°W 85°W 80°W 75°W
10 20 30 40 50 60 70 80 90 100 h
2 4 6 8 10 12 14 16 18 20 h
1 2 3 4 5 6 7 8 9 10 h

1150

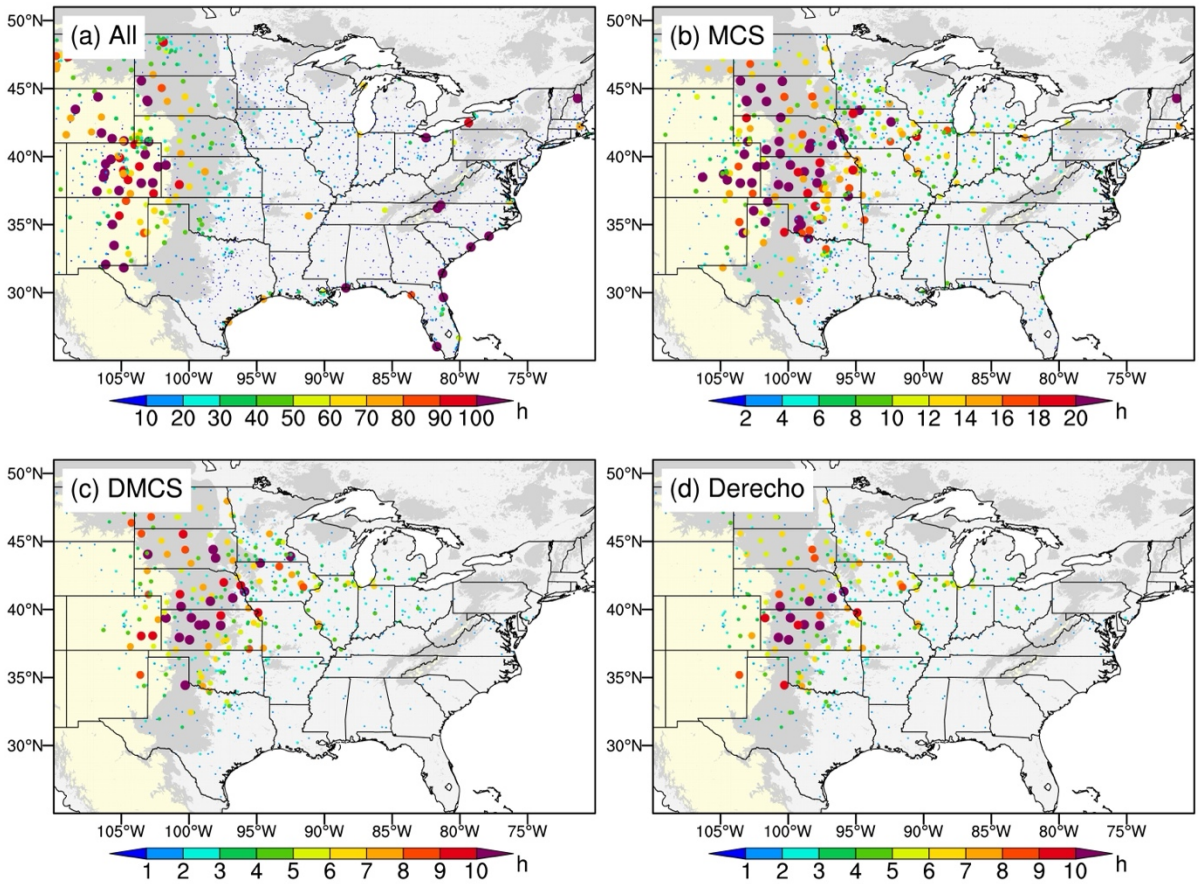

Figure S2. Same as Figure ~~13~~12, but the frequencies of damaging gust occurrences from mesoscale convective system (MCS), derecho~~,~~-producing MCS (DMCS), and derecho ~~feature (DF)~~ are shown in (b), (c), and (d) instead of fractions. Non-derecho-producing MCS events overlapping with tropical cyclones (TCs) are excluded in (b).

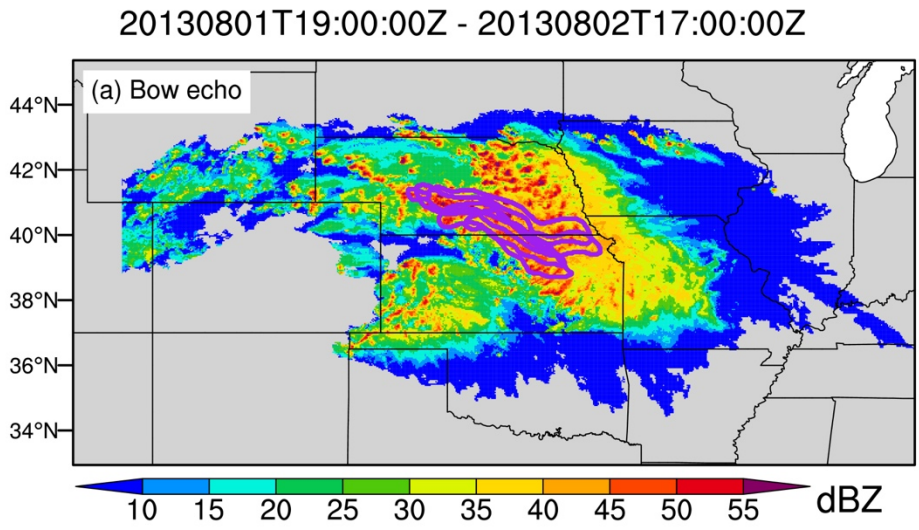
20130801T19:00:00Z - 20130802T17:00:00Z
(a) Bow echo
44°N
42°N
40°N
38°N
36°N
34°N
10 15 20 25 30 35 40 45 50 55
dBZ

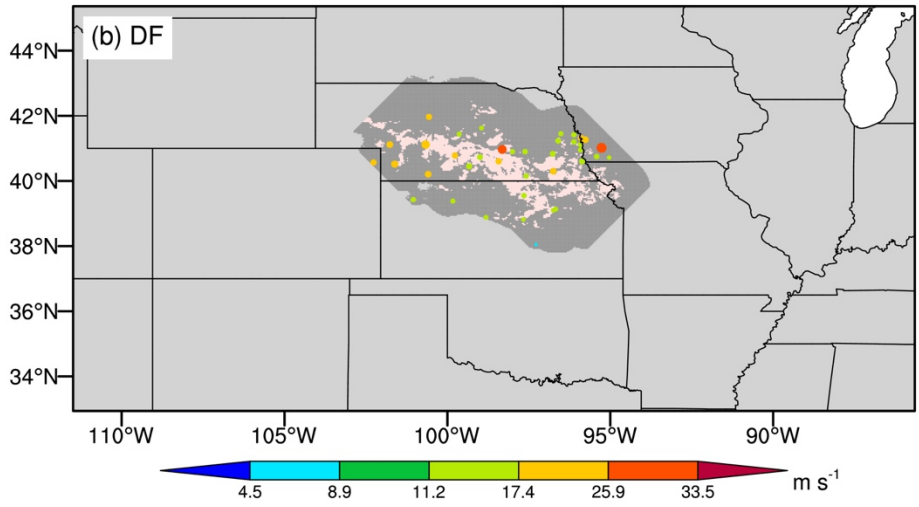
(b) DF
44°N
42°N
40°N
38°N
36°N
34°N
110°W
105°W
100°W
95°W
90°W
4.5 8.9 11.2 17.4 25.9 33.5
m s-1

1157

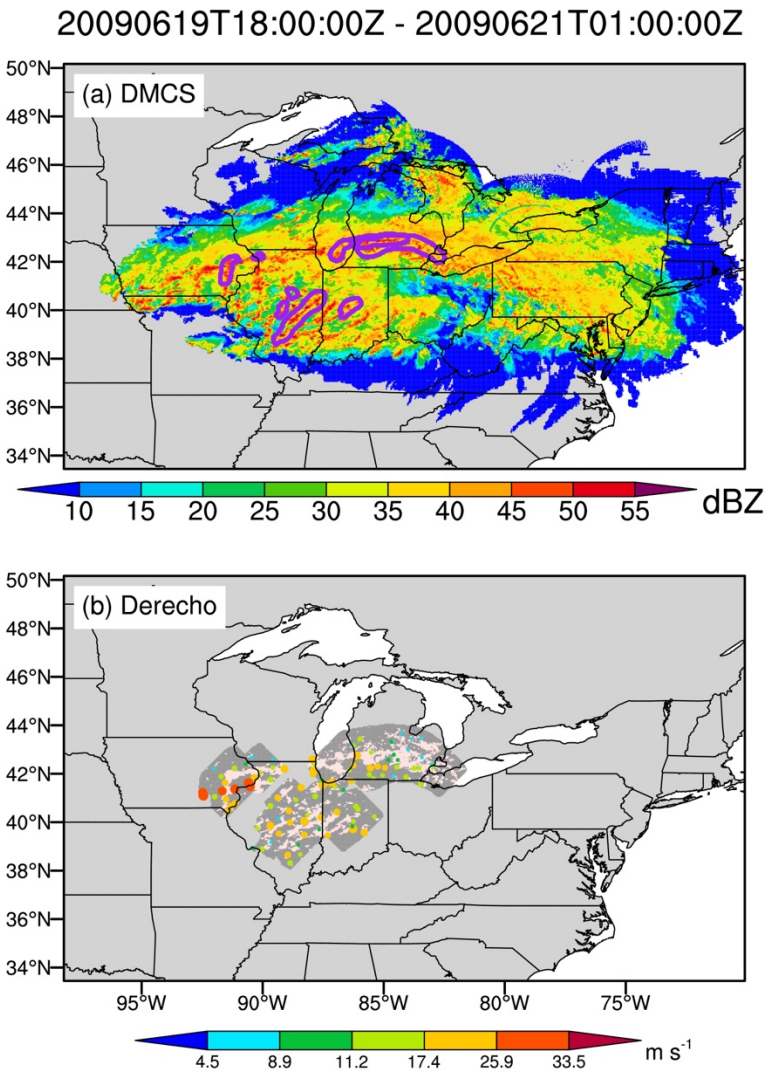

Figure S3. Same as Figure 7 but for an MCS that occurred on ~~1-2 August 2013.~~19-21 June 2009. The automated detection algorithm falsely classifies the MCS as a ~~derecho~~DMCS due to the false identification of bow echoes by the segmentation CNN. The figure title refers to the ~~derecho~~MCS timing range.

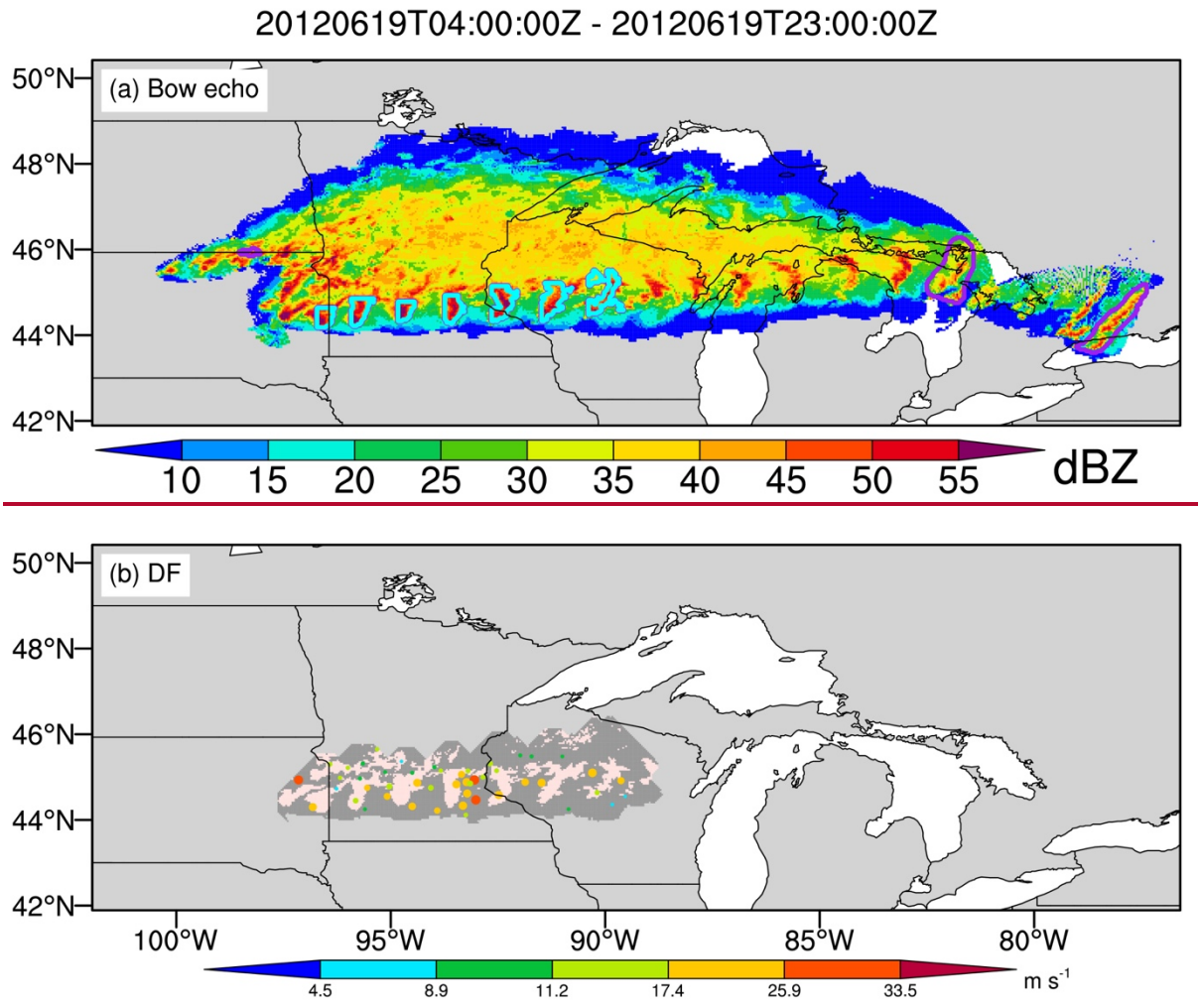
20120619T04:00:00Z - 20120619T23:00:00Z
(a) Bow echo
50°N
48°N
46°N
44°N
42°N
10 15 20 25 30 35 40 45 50 55
dBZ
(b) DF
50°N
48°N
46°N
44°N
42°N
100°W
95°W
90°W
85°W
80°W
4.5 8.9 11.2 17.4 25.9 33.5
m s-1

1163

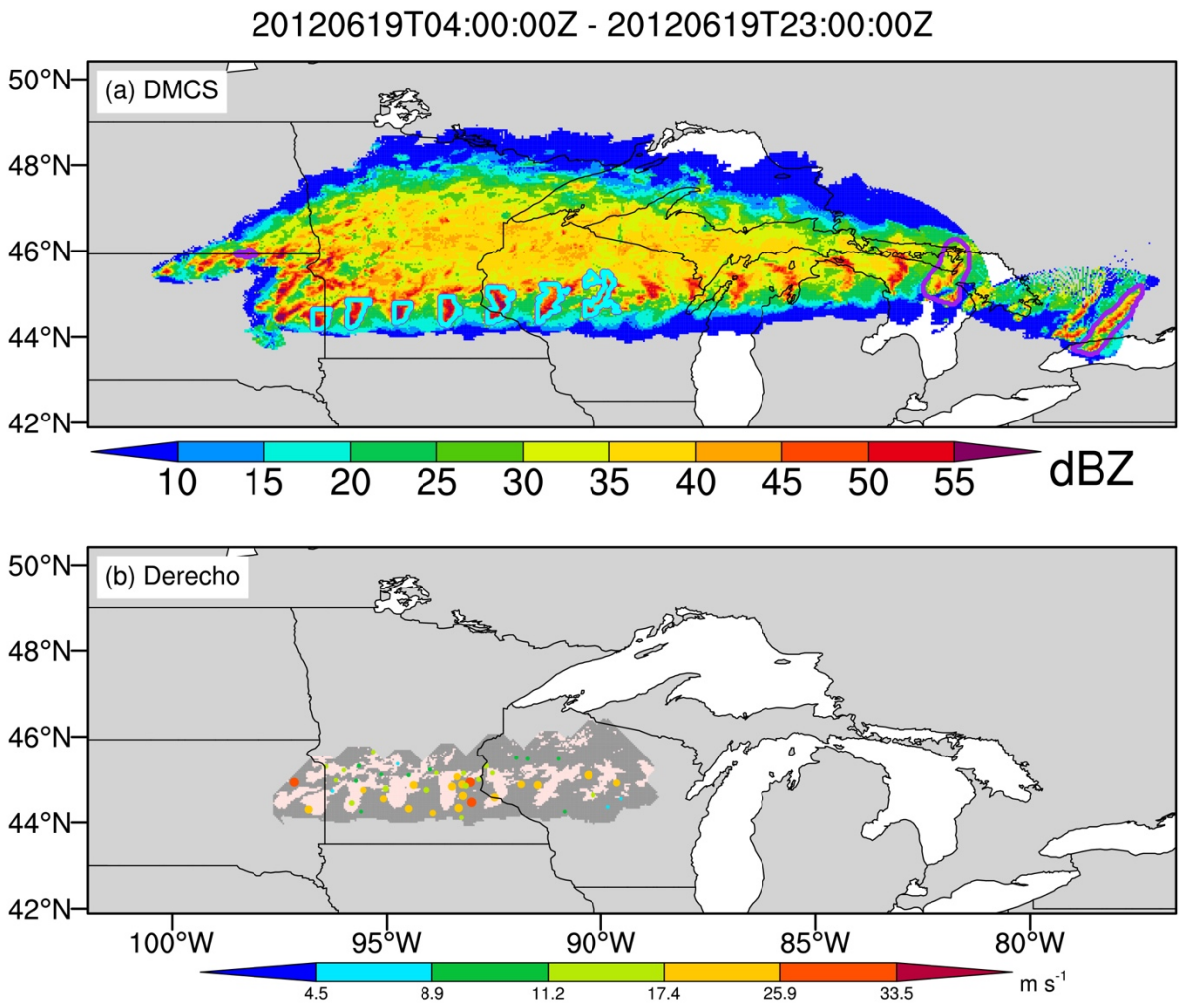

Figure S4. Same as Figure S3 but for a ~~derecho~~DMCS that the automated detection algorithm misses due to a failure in bow echo identification. In (a), purple contours denote CNN-identified bow echoes, while cyan contours refer to bow echoes labeled manually.

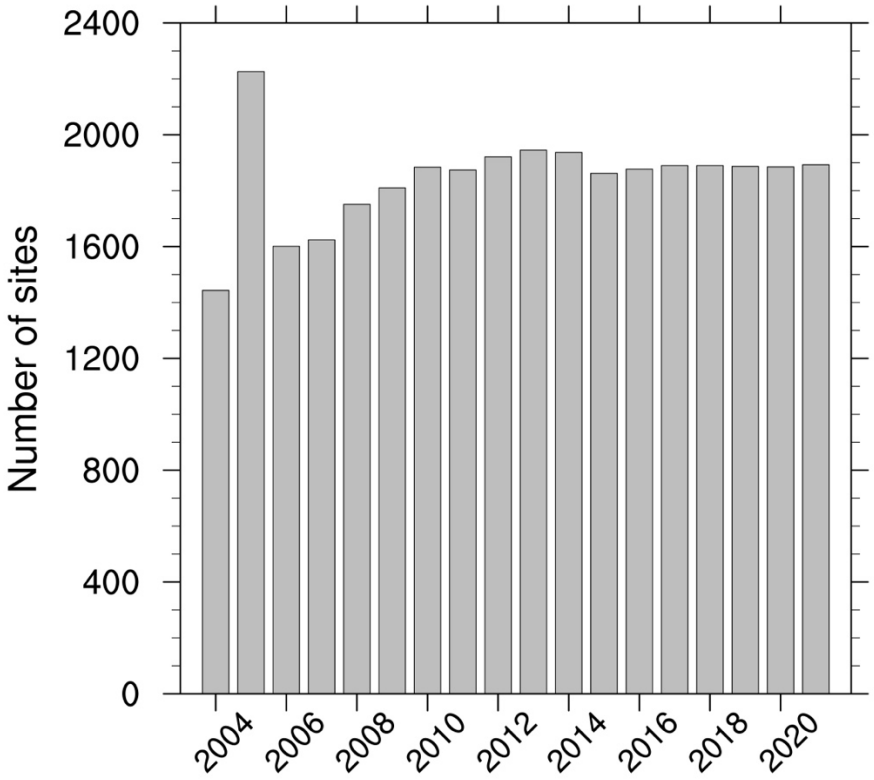

Figure S5. The annual number of ISD gust speed observational sites used in the derecho identification between 2004 and 2021.

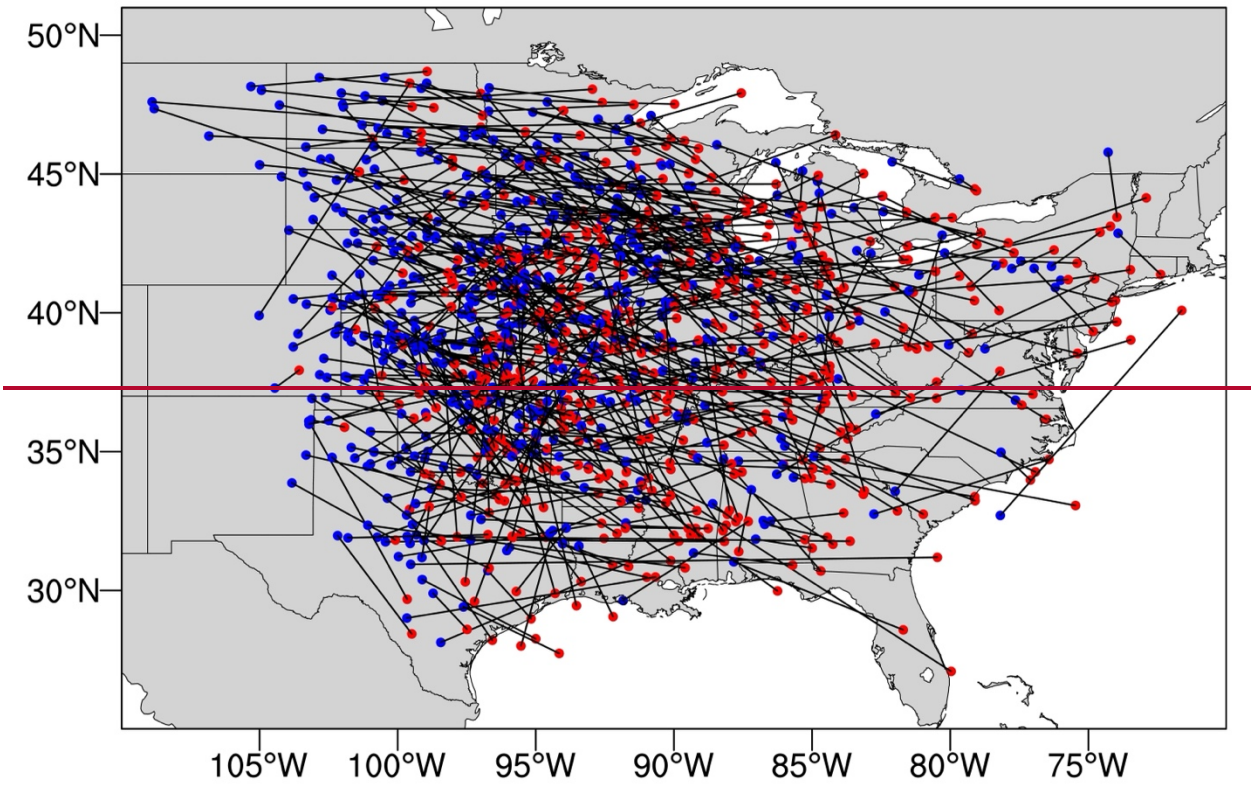

~~Figure S6. The derecho paths (black lines) during their DF periods. Each blue dot denotes the location of a derecho at the beginning of its DF period, while the corresponding red dot refers to the location at the end of the DF period. The location is calculated as the mean latitude and longitude of all grid cells within the DF area and covered by the derecho at the given time. Only grid cells with $Z_{Hmax} \geq 20$ dBZ are considered in the calculation. If there are no grid cells with $Z_{Hmax} \geq 20$ dBZ, we will move to the next hour (for blue dots) or the previous hour (for red dots) until we find grid cells with $Z_{Hmax} \geq 20$ dBZ.~~

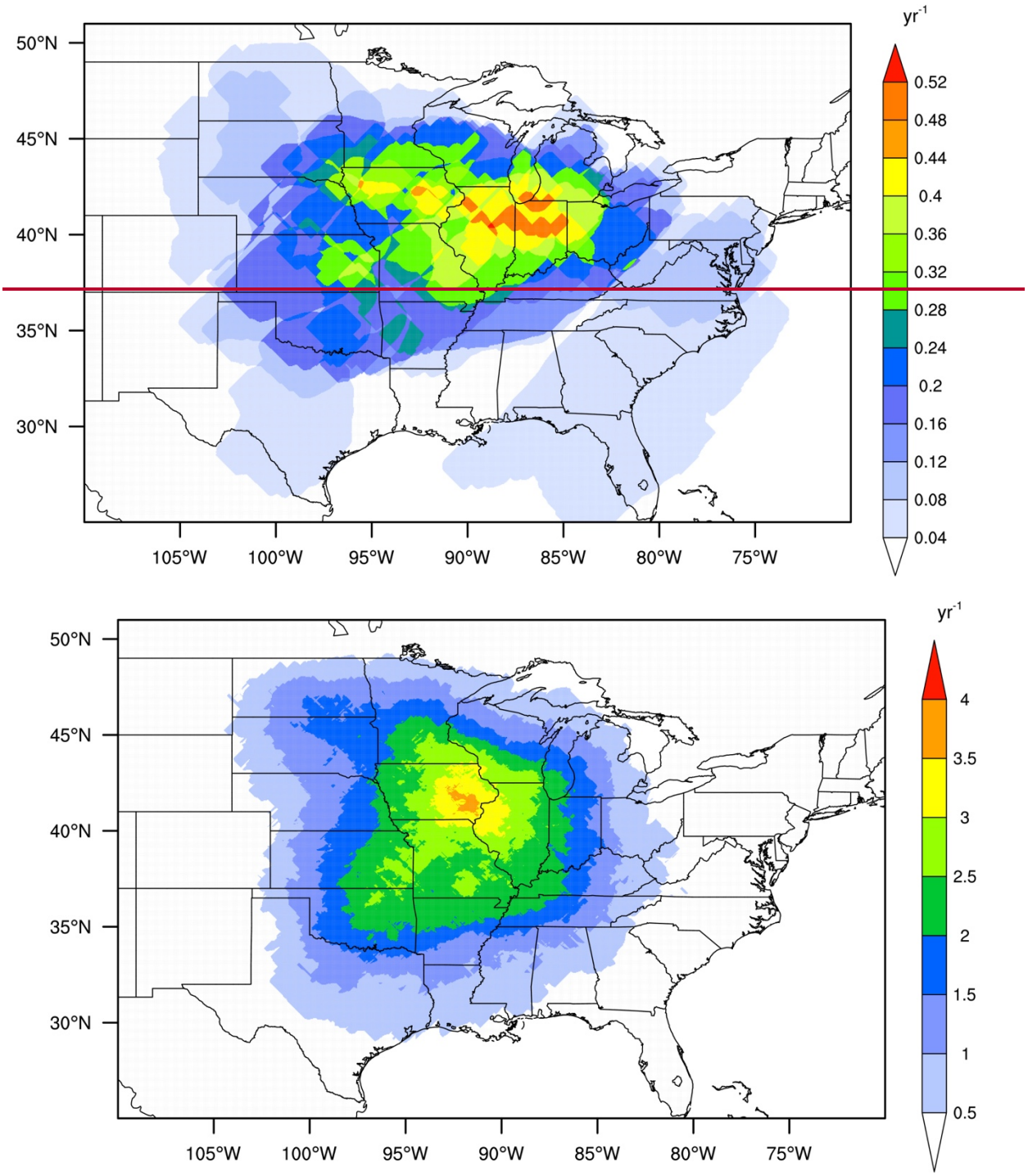

Figure S6. Same as Figure 9 but for the SED-based dataset.

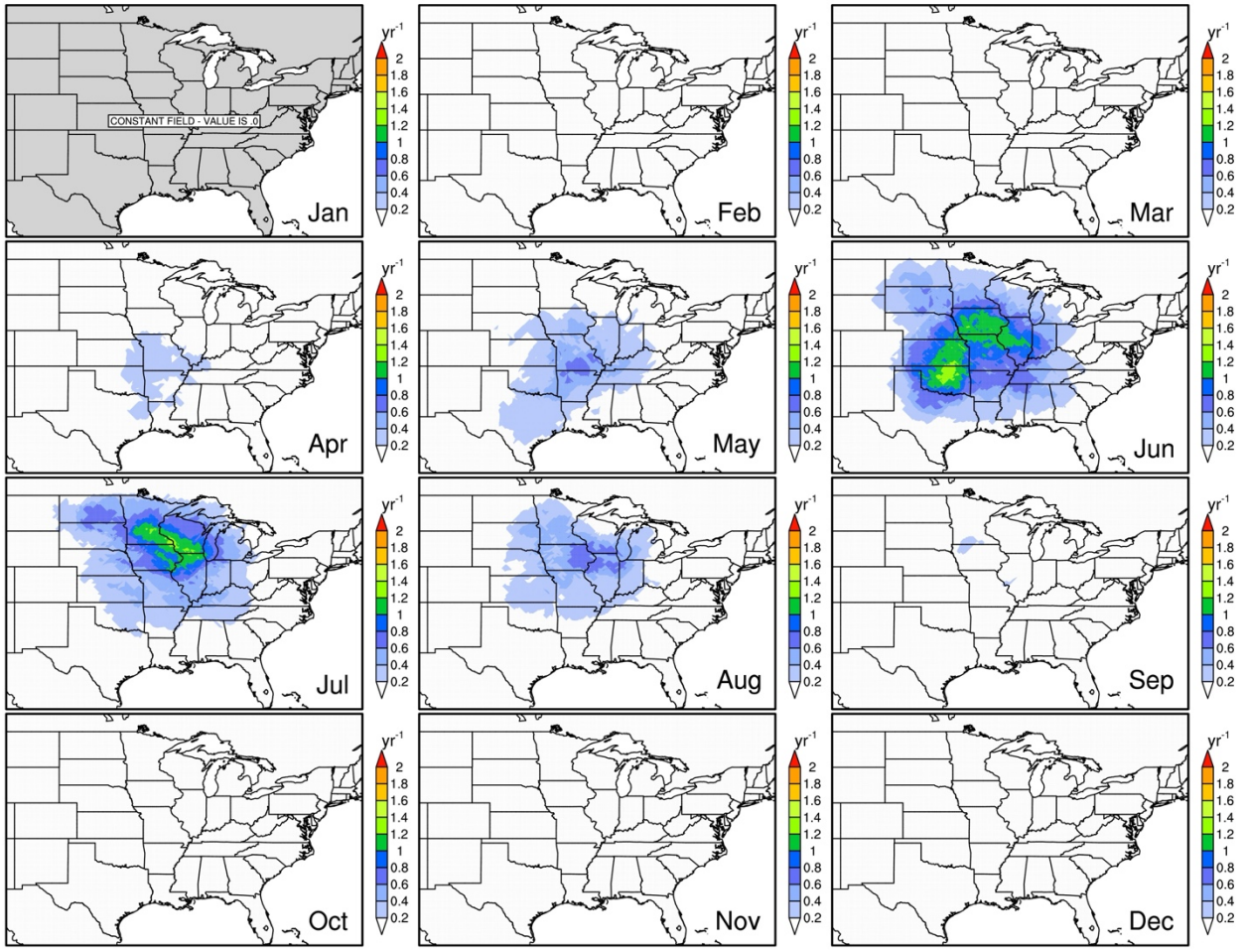

Figure S7. Same as Figure ~~10 but for a sensitivity test with the gust swath calculation based on ≥ 10 sites with damaging gusts. Using the updated criteria, 19~~11 but for SED-based derechos ~~are identified~~.

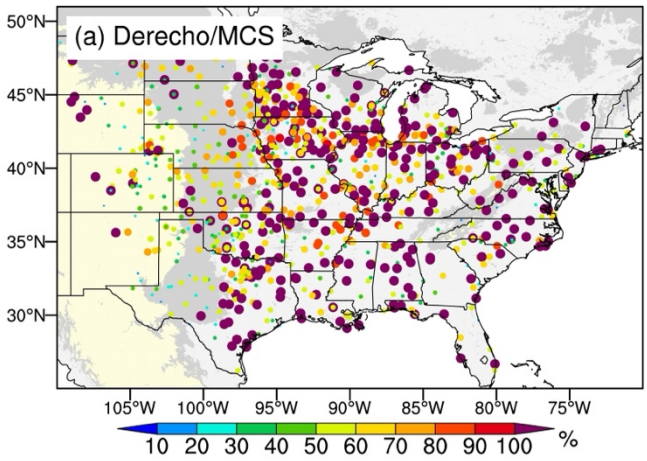
(a) Derecho/MCS
50°N
45°N
40°N
35°N
30°N
105°W 100°W 95°W 90°W 85°W 80°W 75°W
10 20 30 40 50 60 70 80 90 100 %

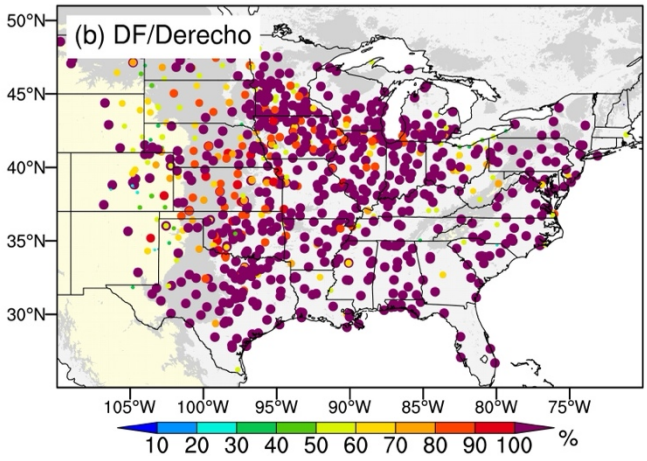
(b) DF/Derecho
50°N
45°N
40°N
35°N
30°N
105°W 100°W 95°W 90°W 85°W 80°W 75°W
10 20 30 40 50 60 70 80 90 100 %

1189

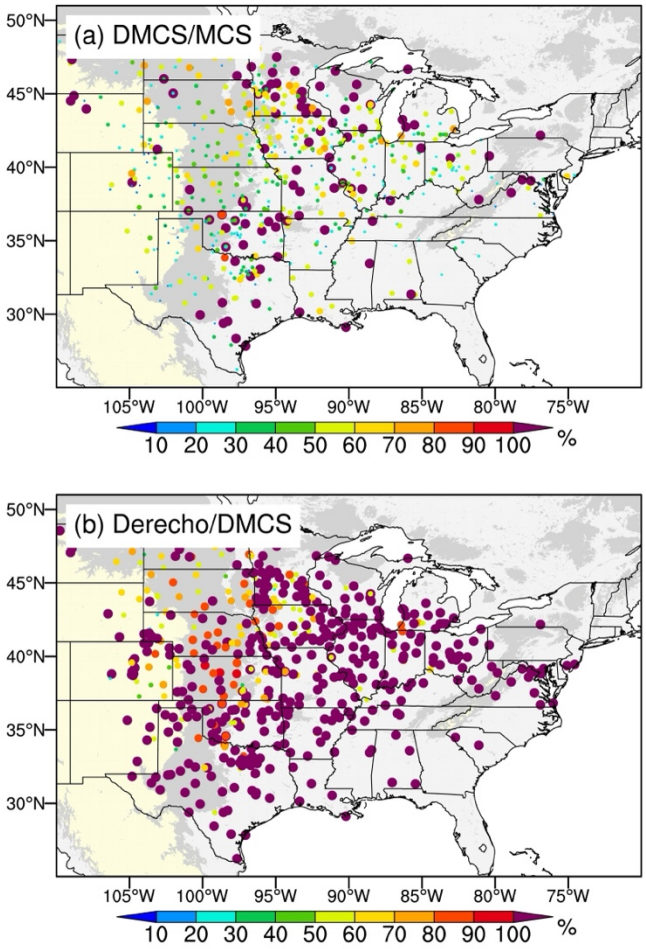

Figure S8. (a) Relative contributions of ~~derecho~~DMCS-associated to MCS-associated ISD damaging gust occurrences between 2004 and 2021 at weather stations over the United States east of the Rocky Mountains. (b) is the same as (a) but for relative contributions of ~~DF-associated to~~ derecho-associated to DMCS-associated damaging gust occurrences. We exclude non-derecho-producing MCS events overlapping with TCs in (a).

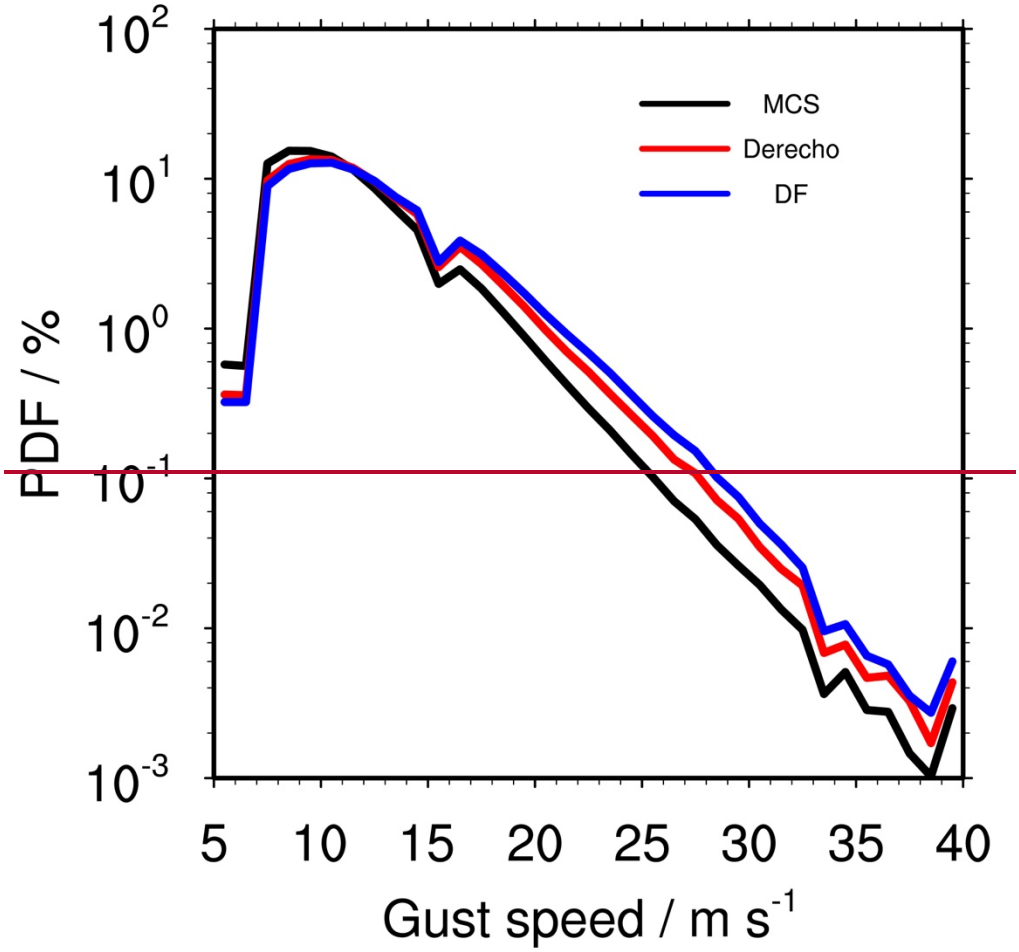
MCS
Derecho
DF
PDF / %
10^{2}
10^{1}
10^{0}
10^{-1}
10^{-2}
10^{-3}
5
10
15
20
25
30
35
40
Gust speed / m s^{-1}

1196

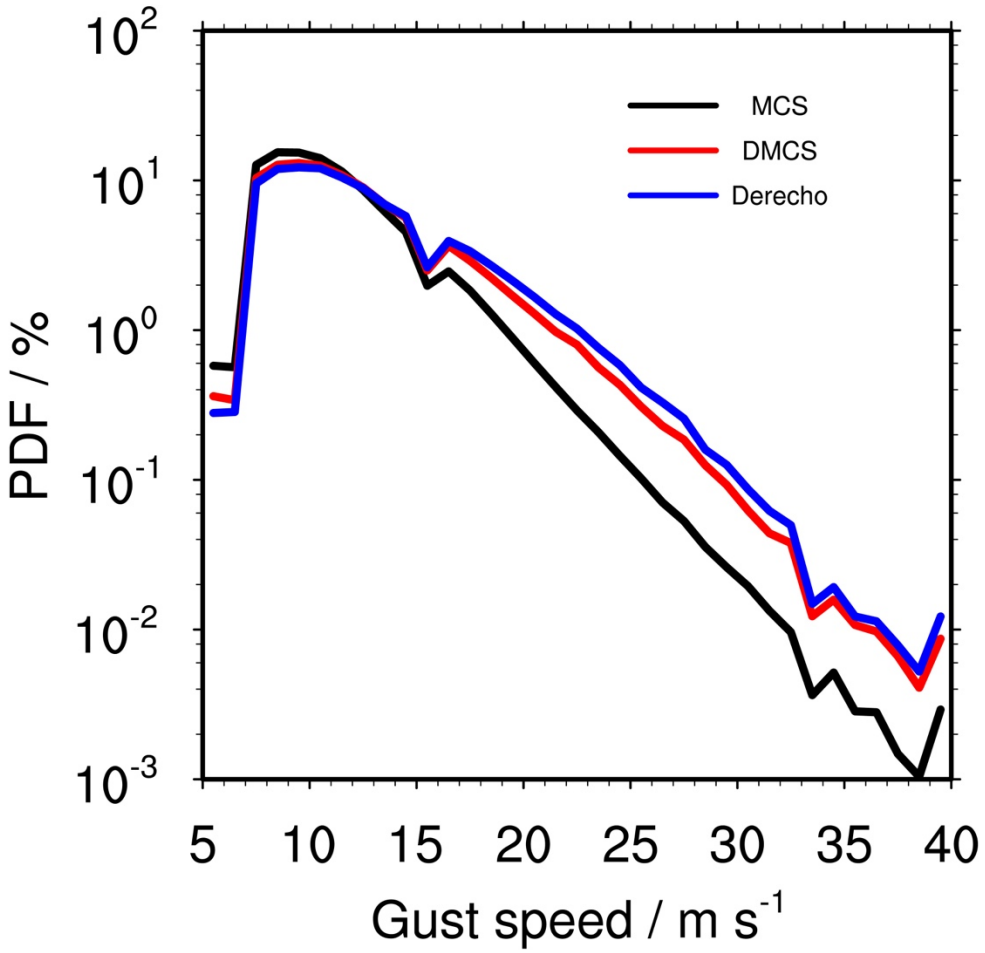

Figure S9. PDFs of land ISD gust speeds associated with MCSs, DMCSs, and derechos~~, and DFs~~ in the United States east of the Rocky Mountains. We exclude non-derecho-producing MCS events overlapping with TCs.

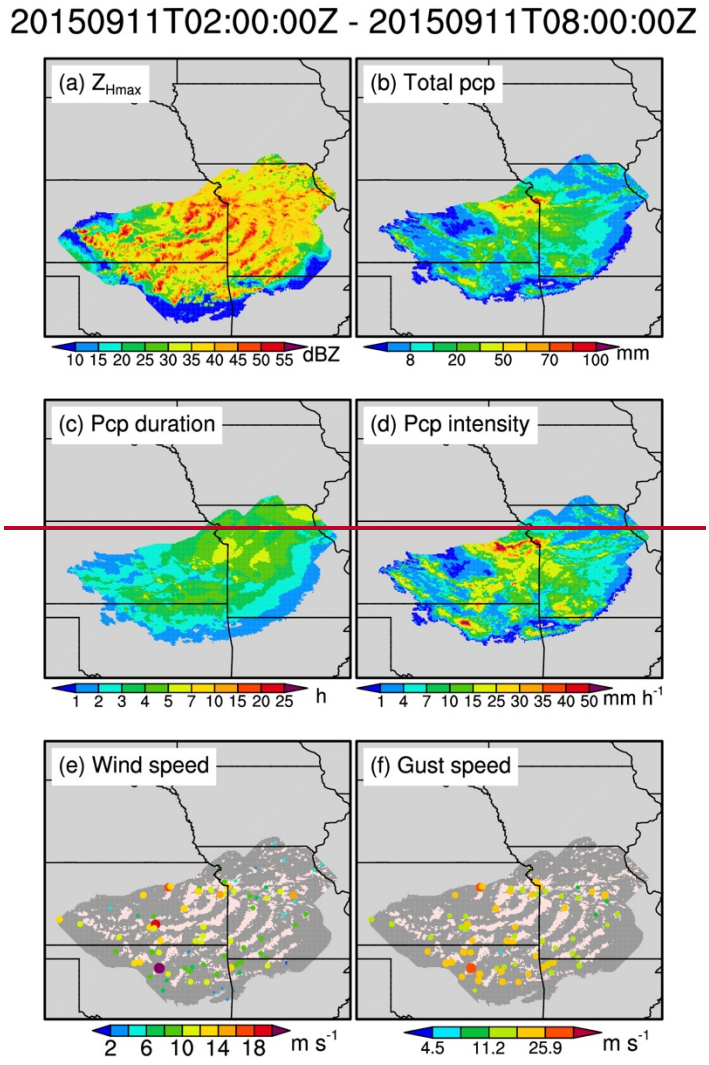
20150911T02:00:00Z - 20150911T08:00:00Z
(a) Z_{Hmax}
10 15 20 25 30 35 40 45 50 55 dBZ
(b) Total pcp
8 20 50 70 100 mm
(c) Pcp duration
1 2 3 4 5 7 10 15 20 25 h
(d) Pcp intensity
1 4 7 10 15 25 30 35 40 50 mm h^{-1}
(e) Wind speed
2 6 10 14 18 m s^{-1}
(f) Gust speed
4.5 11.2 25.9 m s^{-1}

1201

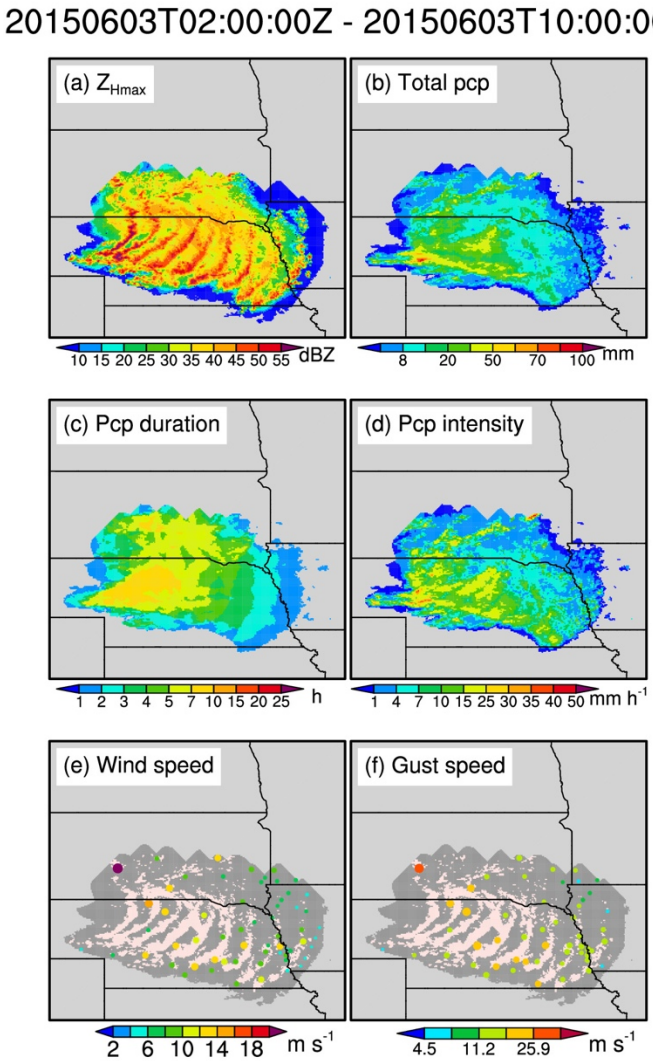

Figure S10. Same as Figure ~~14~~13 but for the spatial evolutions ~~during~~of the accompanying derecho ~~DF period~~. The figure title refers to the ~~DF~~derecho timing range.